DUDLEY KNOX LIBRARY
NAVAL POSTGRADUATE SCHOOL
MONTEREY CA 93943-5101

Approved for public release; distribution is unlimited.

Scattering of Underwater Sound From a Porous Solid Sphere

by

Theodore W. L. Huskey
Lieutenant, United States Navy
B.S., United States Naval Academy, 1986

Submitted in partial fulfillment
of the requirements for the degree of

MASTER OF SCIENCE IN APPLIED SCIENCE

from the

NAVAL POSTGRADUATE SCHOOL
September, 1993

REPORT DOCUMENTATION PAGE

Form Approved OMB No. 0704-0188

Public reporting burden for this collection of information is estimated to average 1 hour per response, including the time for reviewing instruction, searching existing data sources, gathering and maintaining the data needed, and completing and reviewing the collection of information. Send comments regarding this burden estimate or any other aspect of this collection of information, including suggestions for reducing this burden, to Washington headquarters Services, Directorate for Information Operations and Reports, 1215 Jefferson Davis Highway, Suite 1204, Arlington, VA 22202-4302, and to the Office of Management and Budget, Paperwork Reduction Project (0704-0188) Washington DC 20503.

1. AGENCY USE ONLY *(Leave blank)*	2. REPORT DATE	3.REPORT TYPE AND DATES COVERED
	September 1993	Master's Thesis

4. TITLE AND SUBTITLE
SCATTERING OF UNDERWATER SOUND FROM A POROUS SOLID SPHERE

5. FUNDING NUMBERS

6. AUTHOR(S)
Huskey, Theodore, W. L.

7. PERFORMING ORGANIZATION NAME(S) AND ADDRESS(ES)
Naval Postgraduate School
Monterey CA 93943-5000

8. PERFORMING ORGANIZATION REPORT NUMBER:

9. SPONSORING/MONITORING AGENCY NAME(S) AND ADDRESS(ES)

10. SPONSORING / MONITORING AGENCY REPORT NUMBER:

11. SUPPLEMENTARY NOTES
The views expressed in this thesis are those of the author and do not reflect the official policy or position of the Department of Defense or the U.S. Government.

12a. DISTRIBUTION/AVAILABILITY STATEMENT
Approved for public release; distribution is unlimited.

12b. DISTRIBUTION CODE
A

13. ABSTRACT *(maximum 200 words)*

An experiment was performed to measure the scattering of underwater sound from a porous solid for the first time. Two porous solid spheres composed of heat-epoxied glass beads of 100 and 500 micron mean bead diameter were used. The permeability, porosity, and shear modulus of each sample were estimated from measurements made on cylindrical samples which had been manufactured at the same time and of the same glass beads as the spheres. These material properties were used as input to a theoretical model for the sound scattered from a poro-elastic sphere imbedded in a poro-elastic host developed by Kargl and Lim. The experimental data were compared to the theoretical calculations.

Theoretical calculations with 0%, 3%, and 10% skeletal frame damping were compared to experimental data. Very good agreement between measured and predicted scattering was obtained for each sample over certain frequency ranges, taking 10% frame damping in the calculations. For other frequency ranges the agreement was less than good. No systematic trend in the agreement could be discerned with regard to porous grain size or sound frequency.

14. SUBJECT TERMS
Biot, Porous Medium, Backscatter, Borosilicate

15. NUMBER OF PAGES: 73

16. PRICE CODE

17. SECURITY CLASSIFICATION OF REPORT	18. SECURITY CLASSIFICATION OF THIS PAGE	19. SECURITY CLASSIFICATION OF ABSTRACT	20. LIMITATION OF ABSTRACT
Unclassified	Unclassified	Unclassified	UL

NSN 7540-01-280-5500

Standard Form 298 (Rev. 2-89)
Prescribed by ANSI Std. 239-18

ABSTRACT

An experiment was performed to measure the scattering of underwater sound from a porous solid for the first time. Two porous solid spheres composed of heat-epoxied glass beads of 100 and 500 micron mean bead diameter were used. The permeability, porosity, and shear modulus of each sample were estimated from measurements made on cylindrical samples which had been manufactured at the same time and of the same glass beads as the spheres. These material properties were used as input to a theoretical model for the sound scattered from a poro-elastic sphere imbedded in a poro-elastic host developed by Kargl and Lim. The experimental data were compared to the theoretical calculations.

Theoretical calculations with 0%, 3%, and 10% skeletal frame damping were compared to experimental data. Very good agreement between measured and predicted scattering was obtained for each sample over certain frequency ranges, taking 10% frame damping in the calculations. For other frequency ranges the agreement was less than good. No systematic trend in the agreement could be discerned with regard to porous grain size or sound frequency.

Thesis
H957375
c.1

TABLE OF CONTENTS

I. INTRODUCTION.....1

A. BACKGROUND.....1

B. OBJECTIVES.....1

II. HIGHLIGHTS OF SOUND PROPAGATION AND SCATTERING IN POROUS MEDIA.....3

III. SAMPLE PREPARATION AND MATERIAL PROPERTY DETERMINATION.....5

A. DESCRIPTION OF SAMPLES.....5

B. DETERMINATION OF POROSITY.....7

C. DETERMINATION OF PERMEABILITY.....8

D. DETERMINATION OF ELASTIC MODULI.....12

IV. BACKSCATTER EXPERIMENT.....19

A. EXPERIMENT OBJECTIVE.....19

B. EXPERIMENT COMPONENTS.....19

C. LABORATORY TANK SETUP.....21

D. ELECTRONICS.....25

E. EXPERIMENTAL PROCEDURE.....26

V. DATA ANALYSIS AND COMPARISON.....30

A. EXPERIMENTAL RESULTS.....30

B. SOURCES OF THEORETICAL VALUES.....30

C. COMPARISON OF EXPERIMENTAL RESULTS AND CALCULATIONS.....34

DUDLEY KNOX LIBRARY
NAVAL POSTGRADUATE SCHOOL
MONTEREY, CA 93943-5101

D. SPECULATION FOR DISAGREEMENT BETWEEN THEORETICAL AND EXPERIMENTAL VALUES.....40

VI. SUMMARY, CONCLUSIONS, AND RECOMMENDATIONS.....48

A. SUMMARY AND CONCLUSIONS.....48

B. RECOMMENDATIONS.....49

APPENDIX A: EXPERIMENT DATA 100 MICRON SPHERE.....50

APPENDIX B: EXPERIMENT DATA 500 MICRON SPHERE.....57

APPENDIX C: INPUT TO KARGL'S PROGRAM.....61

REFERENCES.....64

INITIAL DISTRIBUTION LIST.....66

ACKNOWLEDGEMENTS

I would like to express my thanks to Ray Lim, Steve Kargl and Doug Todoroff of the Coastal System Station, Panama City, Florida for introducing me to this marvelously intriguing subject. Their patience and assistance during my thesis research is greatly appreciated. I would like to express a special and deeply felt thank you to Professor Steve R. Baker. His confidence in me and faith in my ability to handle this monumental research encouraged me to persevere when confronted with what at times appeared to be insurmountable obstacles. Without his guidance this research would not have been possible.

I. INTRODUCTION

A. BACKGROUND

There has been a resurgence of interest in sound propagation in a fluid-saturated porous medium because of the importance of ocean bottom propagation in a shallow water environment. While sound propagation in a porous medium is not a new subject, the scattering of elastic waves propagating in a porous medium has only recently been considered. An important potential application of this scattering is the acoustic detection of buried mines.

A general theory for the propagation of elastic waves in a porous, fluid-filled medium was derived by Maurice Biot (Biot, 1956a,b, 1962a,b). Biot's theory has recently been applied to the scattering of elastic waves in a porous medium by a compact porous object (Kargl and Lim, 1993). To date, no experiments have been performed to validate this hallmark theoretical application of Biot's theory.

B. OBJECTIVES

The objectives of this research are to measure and compare the scattering of underwater sound waves by a fluid-saturated poro-elastic sphere to theoretical values computed following Kargl and Lim (Kargl and Lim, 1993).

It is noteworthy that this experiment, the scattering of underwater sound from porous solid spheres of glass beads, is the first of its kind.

II. HIGHLIGHTS OF SOUND PROPAGATION AND SCATTERING IN POROUS MEDIA

In a series of papers, Maurice Biot (Biot 1956a,b, 1962a,b) developed a theory for the propagation of elastic waves in a fluid-saturated porous solid. Biot derived equations that describe the interaction between a fluid-saturated porous solid and the fluid in the pores due to the solid's microscopic pore geometry.

The essence of Biot theory is that among the acoustic properties in a fluid-saturated porous solid there exist three propagating body waves: two longitudinal, so called fast and slow compressional waves, and a shear wave. The existence of the slow wave was first confirmed by Plona (Plona, 1980, pp. 259-261). Other measurements have also confirmed the existence of the slow wave (Mayes et. al., 1986, p.249). The slow wave is characterized by 1) the sense of the motion of the fluid and solid are opposite, i.e. "out of phase", 2) it travels with a speed that is slower than the bulk speed of the fluid, and 3) it is typically very lossy. The fast wave is characterized by 1) the sense of the fluid and solid motion are the same, i.e. "in phase", 2) the speed of this wave is between that of the bulk speed of the fluid and the solid, and 3) the

attenuation is small. When we talk about sound propagation in the ocean bottom we are talking about the fast wave. The shear wave can be described as a shear wave that propagates in the porous solid frame with the fluid dragged along by viscous and inertial interaction.

The speed and attenuation of these waves are determined by eleven fundamental material parameters: three material properties of the bulk fluid: 1) mass density, ρ_f, 2) bulk modulus, K_f, and 3) shear viscosity, η, five material properties of the solid scattering object: 1) porosity, P, 2) mass density, ρ_s, 3) bulk modulus of the solid grains, K_s, 4) bulk modulus of the sketal frame, K_b, and 5) shear modulus of the skeletal frame, N, and three parameters that depend upon the microscopic pore geometry: 1) tortuosity, α, 2) permeability, k, and 3) structural factor, δ, in Biot's universal frequency-dependent correction function.

III. SAMPLE PREPARATION AND MATERIAL PROPERTY DETERMINATION

A. DESCRIPTION OF SAMPLES

The porous spheres used as scatters in the experiment are composed of bonded borosilicate glass beads of nominally the same diameter. The unique manner in which the spheres were fabricated is worth discussion.

Many different types of experiments have used consolidated glass beads to simulate sediment (Johnson and Plona, 1982, p. 557). The usual process by which glass beads are consolidated is heat fusion. This method was initially attempted to fabricate the glass bead spheres for the present experiments but proved to be inadequate.

The glass beads were poured into a spherical mold and heated to a temperature of approximately 704 C. The softening temperature of borosilicate is 821 C (Moses, p. 869). The samples were "cooked" for 12 hours. After a cooling period the samples were inspected. It was found that the glass beads had settled, resulting in a sphere-like sample with a smooth spherical lower hemisphere but with a squashed upper hemisphere.

Different temperature and cook-time combinations were investigated in an attempted to reduce the settling. When the cook time was decreased to 8 versus 12 hours, or the

cook temperature reduced a significant amount to 593 C versus 704 C, the degree of settling was reduced. However, the glass beads scarcely adhered to one another, producing very fragile spheres with beads that would crumble off at the slightest touch. When the cook time or cook temperature was increased, the amount of settling increased. There was no cook time and temperature combination that produced a satisfactory sphere.

It was decided to have the samples commercially manufactured by a company experienced in fabricating bonded glass beads (General Polymeric, Reading PA). To make the samples, the glass beads are coated with a fine powder epoxy, then heat fused at a temperature sufficient to activate the epoxy, 150 C. Settling of the glass beads was no problem because the curing temperature was much lower than the softening temperature of the glass beads.

Borosilicate, general purpose, clear glass beads were used to manufacture two spheres. The same mold was used for both. One sphere was composed of glass beads with a mean bead diameter of 100 microns while the other of glass beads with a mean bead diameter of 500 microns. Both spheres had a major and minor axis diameter of 0.066 meters.

Due to the difficulty in measuring the material properties of spherical samples, cylindrical samples of each bead size were prepared at the same time as the spheres.

These samples were 0.151 meters long and 0.052 meters in diameter.

B. DETERMINATION OF POROSITY

The ratio of the open pore volume, the volume not occupied by glass, to the total volume of the sample (sphere or cylinder) is its porosity, *P*.

$$P = \frac{open\ pore\ volume}{total\ volume} \qquad (3.1)$$

The porosity of the cylinders was determined as the ratio of the weight of the cylindrical porous sample to the calculated weight of the sample if were solid borosilicate glass. The porosity of each is listed in Table 3.1.

TABLE 3.1 POROSITIES OF THE TWO CYLINDERS AND THE VALUES USED IN THEIR CALCULATIONS

Sample	100 μ	500 μ
Sample Length, L	0.151 m	0.151 m
Sample Diameter, d	0.052 m	0.052 m
Sample Volume, V	331.13 cm^3	327.32 cm^3
Density of Glass Beads, ρ_g	2231 kg/m^3	2231 kg/m^3
Calculated Mass, M_c	0.738 kg	0.730 kg
Actual Mass, M_a	0.510 kg	0.495 kg
Porosity, P	0.309	0.321

C. DETERMINATION OF PERMEABILITY

Permeability, k, is a measure of the ease with which a porous solid allows fluid to flow through it. It is proportional to the square of the nominal pore radius. Permeability is related to the DC flow resistance of a fluid saturated porous solid. DC flow resistance, R_{DC}, is the average gradient in fluid pressure, ∇p, in the porous solid divided by the average fluid velocity, dU/dt in the direction of the gradient (Baker, 1986,p. 34), and is given in Equation 3.2.

$$R_{DC} = - \frac{\nabla p}{\partial U / \partial t} \qquad (3.2)$$

In terms of the permeability k,

$$R_{DC} = \frac{P \eta}{k} \qquad (3.3)$$

where P is the porosity and η is the fluid shear viscosity. Note that, unlike the DC flow resistance, the permeability is a property of the microscopic geometry of the porous solid only, independent of the filling fluid.

The permeability for each sphere was experimentally determined by the constant head permeability test (Means and Parcher, 1986, pp. 407-417). In the constant head permeability test the volume of water that passes through the porous sample over a period of time, along with the sample's dimensions, is used to calculate a coefficient of permeability, k', with units of meters per second (The symbol k' is being used instead of k for Means and Parcher's coefficient of permeability to avoid any confusion with permeability defined previously)

Figure 3.1, adapted from Means and Parcher, *Physical*

Properties of Soils, Charles E. Merrill Inc., Columbus, Ohio (1964), illustrates the constant head permeameter used to collect the data.

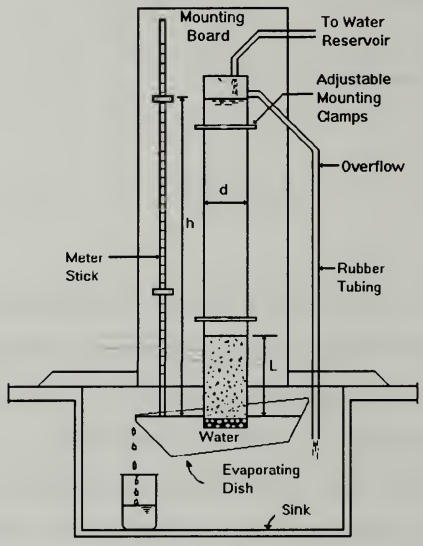

Figure 3.1. Constant Head Permeameter

The cylindrical samples of length *L* and diameter *d* were securely wrapped in "plumber's tape" and connected to one end of a lucite tube using a rubber gasket. The entire apparatus was attached to a lab stand over a sink. A constant supply of tap water was applied to the top of the lucite tube. Once the desired water column height was

established, a constant head was maintain through the use of an overflow tube. After a sufficient period of time had elapsed, ensuring the sample was thoroughly saturated, the volume of water that passed through the sample over a period of time was measured.

Equation 3.4 is used to compute the coefficient of permeability, k'

$$k' = \frac{QL}{tAh} \tag{3.4}$$

where Q is quantity of water collected, L is sample length, t is time required to collect the water, A is area of the sample and h is the distance between the bottom of the sample and the height of the water in the lucite tube.

To get a value of permeability in mks units (m^2), the coefficient of permeability must be multiplied by the conversion factor

$$\frac{\eta}{\rho g} = 1.02 \times 10^{-7} \tag{3.5}$$

where η is the shear viscosity of water (0.001 Pas), g is the acceleration of gravity and ρ is the density of the water (998 kg/m^3)(Baker, 1986, P. 33). Table 3.2 contains

the experimentally determined values used to compute the coefficient of permeability, k', of each sample along with the permeability, k.

TABLE 3.2. CONSTANT HEAD PERMEABILITY DATA

Sample	100 μ	500 μ
Time, t	600 s	240 s
Head, h	0.401 m	0.440 m
Area, A	2.18×10^{-3} m^2	2.18×10^{-3} m^2
Sample Length, L	0.1517 m	0.1517 m
Quantity, Q	2.21×10^{-4} m^3	8.52×10^{-2} m^3
Coeff of Permeability, k'	6.40×10^{-5} m/s	5.61×10^{-4} m/s
Permeability, k	6.53×10^{-12} m^2	5.74×10^{-11} m^2

D. DETERMINATION OF ELASTIC MODULI

The last two parameters determined experimentally were the shear and bulk moduli. The resonant acoustic method was used to determine the elastic moduli of the cylindrical samples (Garrett, 1990). The resonant acoustic method is

based on the notion that a uniform cylinder, with a cross section of diameter d and of length L which is significantly greater than the diameter, will propagate three independent waves (longitudinal, torsional, and flexural) if their wavelengths λ are much greater than the diameter d. These modes will exhibit resonance at frequencies that depend upon the length and the boundary conditions at the ends of the rods.

In the classic resonant acoustic experiment a long cylindrical rod is selectively excited in its torsional, longitudinal, and flexural modes using a single pair of electrodynamic transducers consisting of coils glued to each end of the bar and placed in the field of a magnet. See Garrett for a through discussion of the experiment (Garrett, 1990).

The previously introduced porous cylindrical rods were prepared for this measurement in a similar fashion. The transducer coils were 20 windings of magnet wire, approximately one meter in length, epoxied to each end of the rods. Particular attention was paid to limiting the amount of epoxy used so as to minimize the mass loading of the bar ends by the transducers. The total mass of each pair of coils and the epoxy used to adhere it to the rod was 5.15 grams. Since the mass of the 100 micron sample was 510.41 grams and the mass of the 500 micron sample was

495.23 grams, any mass loading caused by the coils and epoxy is considered negligible.

The optimum sample aspect ratio, L:d, for the acoustic resonant experiment is on the order of 20:1 (Garrett, 1990, p. 212). The two porous cylinder samples have aspects ratios of approximately 3:1. As a result, several apparatus modifications were necessary.

The major impact of the relatively small aspect ratio was excessive electrical crosstalk between the two end coils due to magnetic flux coupling. Two modifications were made to reduce the crosstalk as much as possible. The first modification was to the alignment of the cylindrical rod's two transducer coils. Normally the coils are oriented with their planes parallel to one another. To reduce the coupled magnetic flux, the planes of the coils were instead oriented 90 degrees with respect to each other. The second modification was to wrap a moveable "humbucking" coil around the middle of the cylinder. The position of and drive level to this coil were adjusted to null out as much of the crosstalk as possible.

Each cylindrical rod was placed with its axis at the center of the pole-piece faces, which were aligned along the bar axis. Figure 3.2, from Garrett, "Resonant Acoustic Determination of Elastic Moduli," *J. Acoust. Soc. Am.* **88**, 213 (1990), shows the magnet/rod configuration at each end.

Figure 3.3 illustrates the positioning of the coils with respect to the magnet pole pieces.

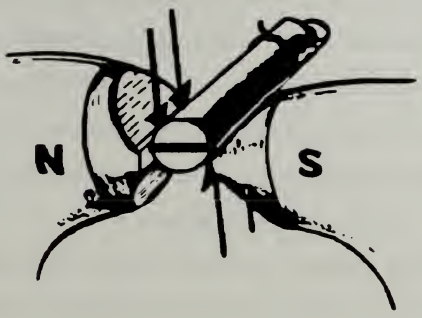

Figure 3.2. Position of the Transducer Coils Relative to the Magnet's Pole Pieces for the Torsional Modes.

Figure 3.3. Modified Rod and Magnet Configuration for the Acoustic Resonant Experiment.

The acoustic resonant experiment can be used to determine all three resonant modes, torsional, flexural and longitudinal, of a long thin sample rod. Although attempts were made to observe all three modes, due to the excessive electrical crosstalk, only the torsional mode was observable. For both the 100 micron and 500 micron samples only the first and second harmonic modes were observable. For these it was possible to measure only their resonance frequency, not their quality factor.

The first and second harmonic modes were observed in both the 100 micron and 500 micron samples. The shear modulus N was computed using equation 3.6:

$$N = 4\rho L^2 (f_n/n)^2 \qquad (3.6)$$

where L is the length, f_n is the frequency of the nth mode, n is the mode number, and ρ is the mass density of the rods. ρ is computed using equation 3.7:

$$\rho = (1 - P)\rho_s \qquad (3.7)$$

Where ρ is the bulk mass density of the glass beads. The shear modulus for each sample is listed in Table 3.3.

Since the longitudinal modes were not observable, the

bulk modulus had to be estimated using the shear modulus and Poisson's ratio. Equation 3.8 shows the relationship between the Poisson's ratio, ν, and the shear, N, and bulk, K, modulus of a material.

$$\nu = \frac{3K - 2N}{2(3K + N)} \qquad (3.8)$$

The exact value of Poisson's ratio for the sample rods is not known. Poisson's ration for the borosilicate glass, of which the beads are made, is 0.20 (Moses, p. 869). There was some concern as to whether Poisson's ratio for a porous rod composed of borosilicate beads should be the same as bulk borosilicate. It was noted that Berryman's effective medium calculation of the elastic moduli for the porous solid samples, which is based upon input elastic moduli for borosilicate, and which is used by Kargl and Lim, yields a Poisson's ratio of 0.20 for the porous sample. Accordingly, a Poisson's ratio of 0.20 was assumed in calculating the bulk modulus for the porous solid samples from the measured shear modulus. The bulk and shear moduli for each sample are listed in Table 3.2.

TABLE 3.2. POROUS SAMPLE SHEAR AND BULK MODULI

Sample	100 μ	500 μ
Sample Density, ρ	1541 kg/m^3	1513 kg/m^3
Mode Frequency, f_n	n=1 4460 Hz	n=2 4405 Hz
	n=2 8900 Hz	n=2 8900 Hz
Shear Modulus, N	n=1 2.82x10^9 Pa	n=1 2.70x10^9 Pa
	n=2 2.81x10^9 Pa	n=2 2.75x10^9 Pa
Average Shear	2.81x10^9 Pa	2.72x10^9 Pa
Bulk Modulus, K assuming ν=0.20	14.07x10^9 Pa	13.62x10^9 Pa

IV. BACKSCATTER EXPERIMENT

A. EXPERIMENT OBJECTIVE

The backscattering experiment involved measuring the amplitude of the backscattered acoustic pressure from a porous solid sphere in water.

B. EXPERIMENT COMPONENTS

The backscatter experiment consisted of four major components: 1)a water-filled tank, 2)scattering objects (porous spheres), 3)an acoustic projector, and 4)an acoustic receiver (hydrophone). The experiment was conducted in a water-filled laboratory tank that was 7.32 meters in length, 1.64 meters in width and 2.02 meters in depth. All tank boundaries, except the top surface, were covered with sound absorbing tiles. The scattering objects were the previously discussed porous spheres 6.64 centimeters in diameter.

The acoustic projector was a type F33 general purpose directional transducer composed of two concentric arrays of piezoelectric vibrators (USRD Transducer Catalog 1991). Figure 4.1 is an illustration, from the *USRD Transducer Catalog*, April 1991, of the type F33 transducer. The inner array consists of 12 PZT disks that form a 3.8 by 5.0 centimeter rectangle. The frequency range of the inner

array is 15-150 kHz. The outer array consists of 64 PZT disks that form a 20.8 by 21.7 centimeter rectangle. The frequency range of the outer array is 1-150 kHz.

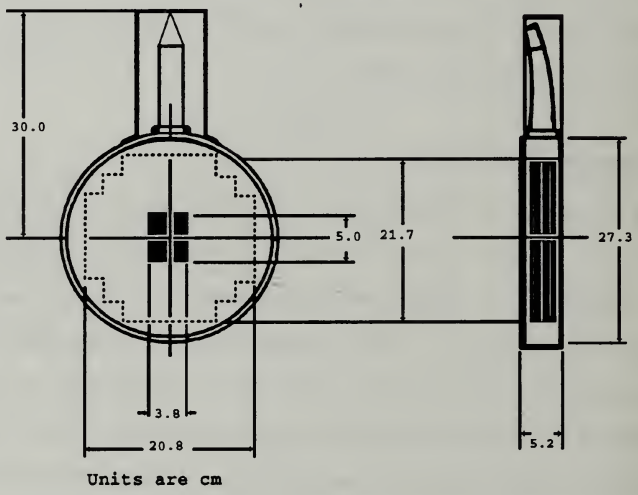

Figure 4.1 Type F33 General Purpose Directional Transducer.

The acoustic receiver was a Bruel and Kjaer type 8103 miniature hydrophone. The type 8103 is illustrated, from its calibration chart, in Figure 4.2. It has an operating range of 0.1-180 kHz, is 2.5 centimeters long, has a radius of 0.475 centimeters.

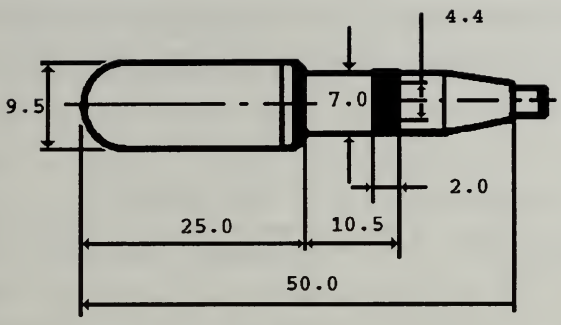

Figure 4.2 Bruel & Kjaer Type 8103 Miniature Hydrophone.

C. LABORATORY TANK SETUP

In order to compare the backscatter data to Kargl and Lim's theory, it was necessary to ensure that far-field conditions were met for the scatterer and the hydrophone (Kinsler et. al., p. 188). Equation 4.1 was used to compute the far-field distance, r,

$$r = \frac{d^2}{\lambda} \qquad (4.1)$$

where d is the source diameter and λ is the source wavelength. The values computed for radiation from the inner and outer arrays of the F33, and from the spherical scatters, are listed in Table 4.1 for the worst case frequency of 150 kHz.

TABLE 4.1 FAR-FIELD DISTANCE

Component	Spheres	Inner Array	Outer Array
Diameter, d	6.64 cm	5.00 cm	27.10 cm
Wavelength, λ @ 150 kHz	1.00 cm	1.00 cm	1.00 cm
Far-Field Distance, r	0.44 m	0.25 m	7.32 m

Upon examination of Table 4.1 it is clear that the far-field distance for the F33 outer array exceeds the dimensions of the tank. For this reason the inner array was used as the projector. The components, projector, sphere and hydrophone were arranged in a configuration that satisfied all far-field criteria.

Figure 4.3 is an illustration of the tank and components configuration. The projector was position at one end of the tank, 1.01 meters below the surface, 0.82 meters from the sides, facing down the center of the tank. Prior to being

placed in the tank, the sphere being investigated was secured in a hairnet, placed in a beaker full of water from the tank, and vacuum degassed. This was necessary to ensure the sphere was as completely water-saturated as possible. The sphere was then lowered into the tank, still in the beaker full of water. It was then suspended from a nylon string attached to the hairnet 1.01 meters below the surface, on axis with the projector, 1.14 meters from the projector. The miniature hydrophone was the only component that did not remain at one location throughout the experiment.

The hydrophone was positioned by suspending it from a "hula-hoop", which was secured, concentric with the sphere, to the grating that covered the tank. The radius of the "hula-hoop" was 0.44 meters and was marked at 10 degree increments to aid in the positioning of the hydrophone. A weight was attached to the lower end of the hydrophone cable by a length of nylon string, with a length such that the weight was positioned centimeters above the tank bottom.

The miniature hydrophone was initially position on axis between the projector and the sphere a distance of 0.44 meters from the sphere. This distance was chosen to ensure that the hydrophone was in the sphere's as well as the projector's far field. During the experiment the hydrophone was moved around the sphere in 10 degree increments.

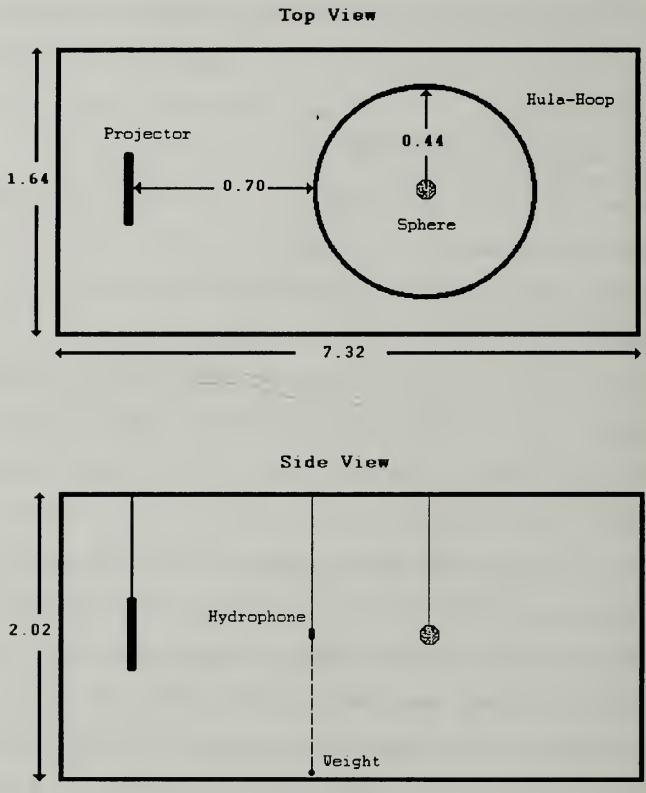

Figure 4.3 Top and Side View of Laboratory Tank Setup.

D. ELECTRONICS

Figure 4.4 is a block diagram of the electronics used in the experiment. The transmitted signal was generated by a Hewlett-Packard Model 3314A Function Generator and amplified by a Hewlett-Packard Model 467A Power Amplifier, then applied to the type F33 transducer. The maximum output voltage the amplifier is 20 volts peak-to-peak. The output of the signal generator was monitored with a Nicolet Model Pro 30 Digital Oscilloscope. The output from the Bruel and Kjaer type 8103 miniature hydrophone was filtered by a Ithaco 1201 Low Noise Preamplifier and input to the Nicolet Digital Oscilloscope for analysis. An Iwatsu SS5710 Oscilloscope was used to monitor the waveforms from the power amplifier (transmitted signal) and the output from the low noise preamplifier (received signal).

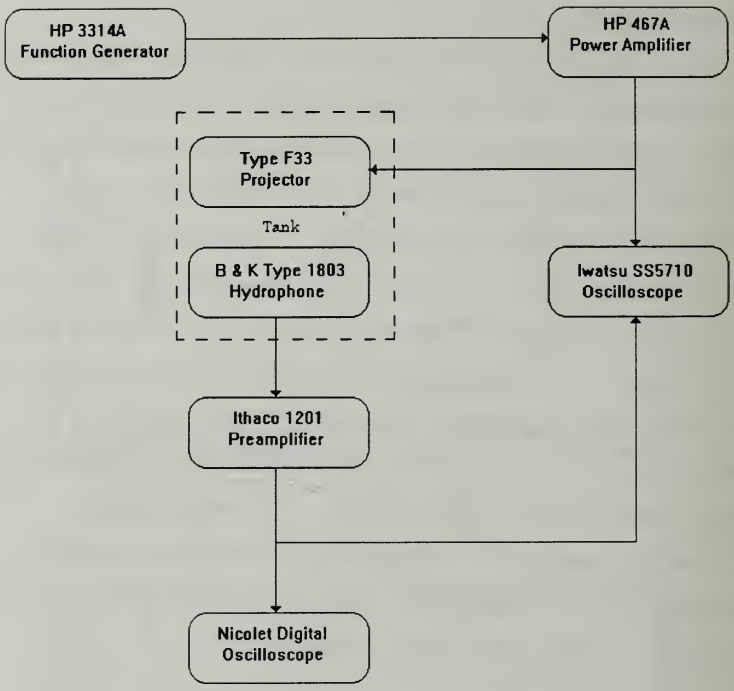

Figure 4.4 Diagram of Electrical Components.

E. EXPERIMENTAL PROCEDURE

Based upon the frequency range of the inner array of the type F33 projector (USRD Catalog 1991), a frequency range of 30 kHz to 150 Khz was used for the backscatter measurements.

Backscatter measurements were taken from 150 kHz down to

30 kHz in 10kHz intervals for the 100 micron sphere and in 30 kHz intervals for the 500 micron sphere. The relatively close proximity of the sphere, projector, hydrophone, and tank boundaries to each other determined the number of cycles (8) that was chosen for the transmitted pulse. Separating the signal of interest from the many boundary reflected signals was difficult at, and impossible beyond, angles of $\pm$ 090 degrees from the 180 degree backscatter direction.

With the hydrophone at its initial position, on axis between the projector and the sphere, the function generator was first set to 150 kHz. The typical voltage applied to the projector was 20 volts peak-to-peak. The filtered scattered signal from the hydrophone was averaged 512 times by the Nicolet digital oscilloscope. Figures 4.5 and 4.6 are typical averaged screen displays from the Nicolet digital osccilloscope. The positive and negative peak values from the averaged signal were recorded, averaged, then added to produce an average peak-to-peak voltage of the scattered return for that particular frequency/bearing combination. Particular care was taken to ensure that the ring-up and ring-down of the signal was not measured as part of the scattered return signal. The frequency of the signal was then decreased either 10 kHz or 30 kHz, depending upon which sphere was being investigated, to the next lower

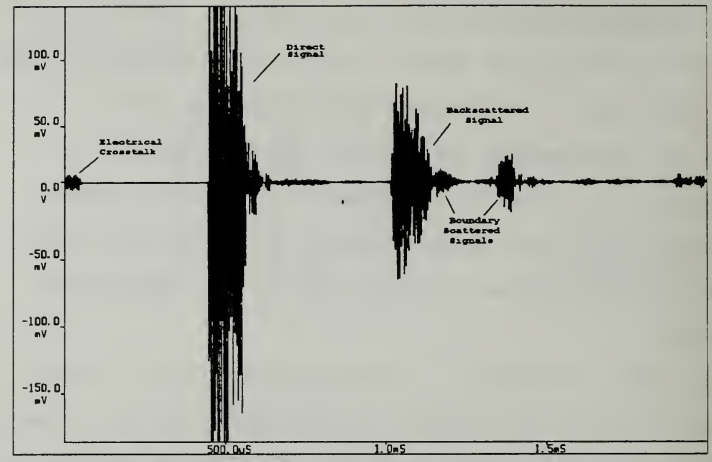

Figure 4.5 Typical Averaged Total Signal Screen Dump

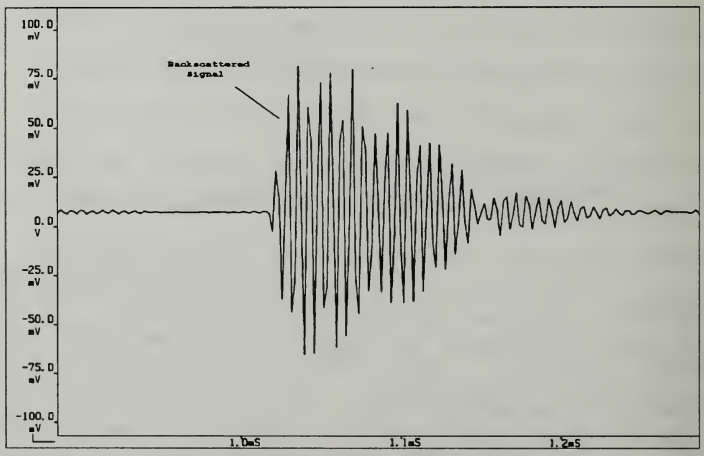

Figure 4.6 Typical Averaged Backscatter Signal Screen Dump

frequency and the scattered return measured. This procedure was continued down to a frequency of 30 kHz. The hydrophone was then moved in 10 degrees increments to the right and the procedure repeated until the data were no longer readable due to boundary interference. The left side was investigated in the same manner. After all the data were collected for the sphere it was lowered to the tank bottom and the hydrophone was positioned in the sphere's normal position. Next, the peak-to-peak values of the pulse incident at the hydrophone were collected over the same frequency range as for the scattering measurements. These peak to peak voltages were used in the normalization of the scattered signals. The peak to peak scattered and incident values for the 100 micron sphere are listed in Appendix A, while the values for the 500 micron sphere are listed in Appendix B.

V. DATA ANALYSIS AND COMPARISON

A. EXPERIMENTAL RESULTS

For comparison purposes, the peak-to-peak backscattered hydrophone output voltage values were normalized by the following equation:

$$Normalized\ Scattering = \frac{V_{scat} \times r}{V_{inc}} \qquad (5.1)$$

where V_{inc} is the peak-to-peak voltage of the incident signal, V_{scat} is the peak-to-peak voltage of the scattered signal, and r is the distance from the scatterer to the receiver, 0.44 m. Spherical spreading of the scattered wave was assumed. The values of the normalized scattering for all data taken are given in Appendix A and B, respectively, for the 100 micron and 500 micron samples.

B. SOURCES OF THEORETICAL VALUES

Theoretical values of scattered pressure were computed for a rigid and massive sphere following Morse (Morse, p. 355) and for a porous sphere using a Fortran program provided by Kargl (Kargl, 1993) based upon Kargl and Lim's application of Biot's theory (Kargl and Lim, 1993).

Kargl's program calculates the scattering of fast and slow compressional waves from a fluid-saturated poroelastic sphere embedded in a fluid-saturated poroelastic host. Due to the versatility of the program, 29 inputs are required. In order to compare results from Kargl's program to the laboratory data for a porous sphere in water, the input parameters for the host porous medium were chosen to simulate water as closely as possible. The input values used are listed in Appendix C.

As a confidence test of Kargl's program, input parameters were chosen to simulate a rigid and massive solid sphere target in water for comparison to known results. A rigid and massive sphere was approximated by a sphere with a density 100 times that of water, with a bulk modulus 10,000 times that of water, and a Poisson's ratio of 1/3. The results of Kargl's program were compared to the scattering of a infinitely rigid and massive sphere in water following Morse (Morse, p. 355) for the frequencies of interest, 30, 60, 90, 120 and 150 kHz. The comparisons are illustrated in Figures 5.1-5. The solid curves correspond to the theoretical values generated by Kargl's program while the dotted curves correspond to theoretical values generated following Morse. The agreement is satisfactory and is taken as validation of Kargl's program.

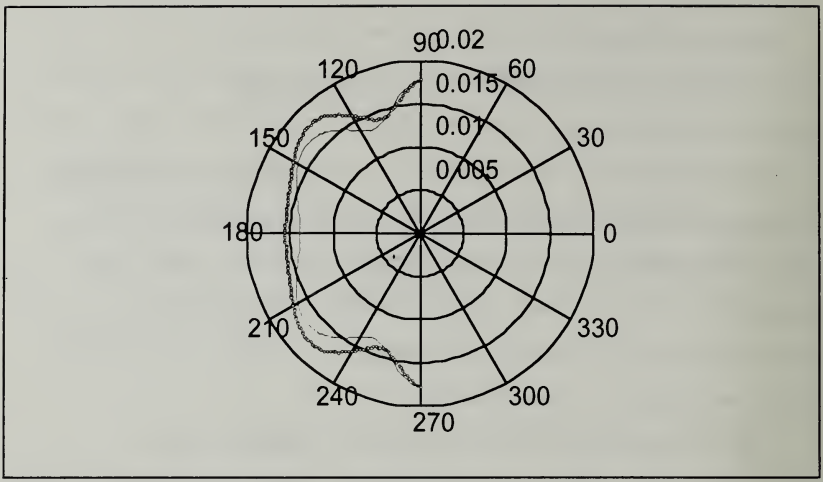

Figure 5.1. Normalized Scattering, 30 kHz Solid Sphere: Morse(o) Kargl(-)

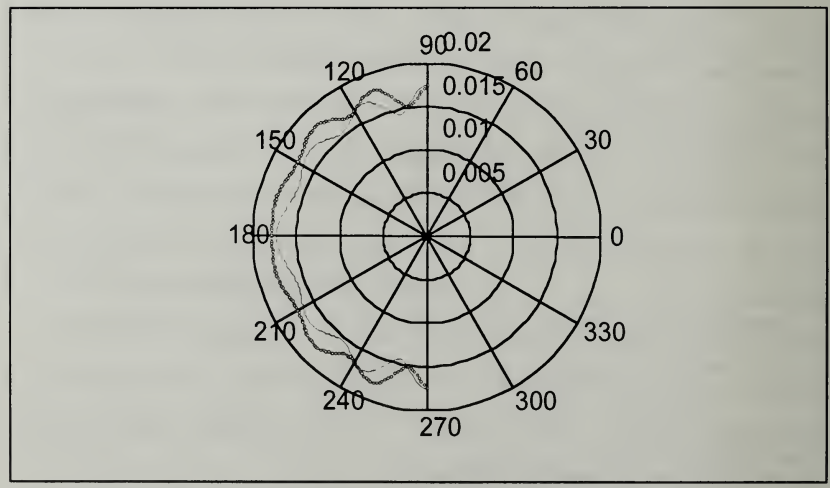

Figure 5.2. Normalized Scattering, 60 kHz Solid Sphere: Morse(o) Kargl(-)

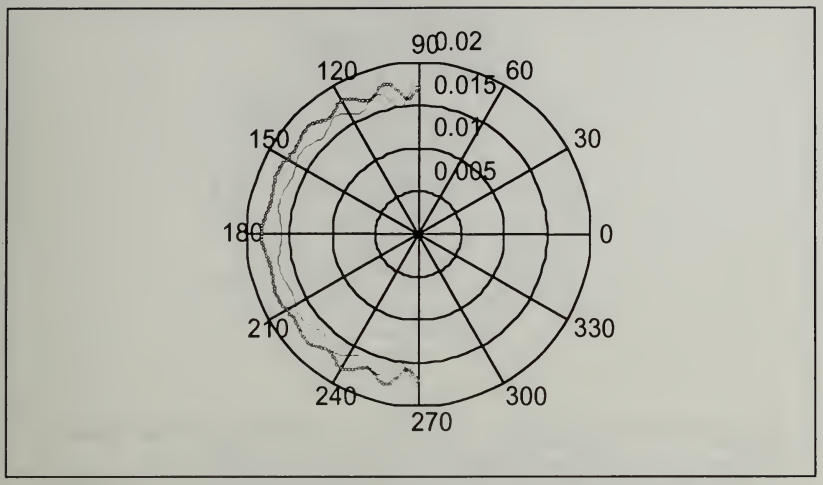

Figure 5.3. Normalized Scattering, 90 kHz Solid Sphere: Morse(o) Kargl(-)

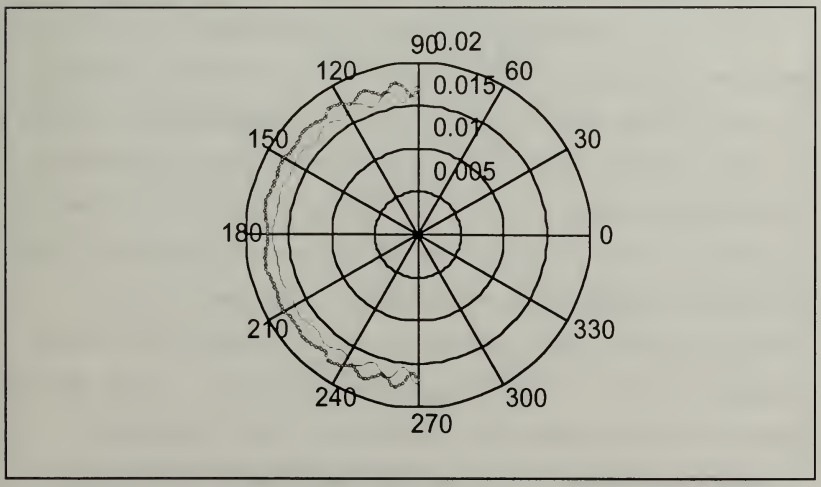

Figure 5.4. Normalized Scattering, 120 kHz Solid Sphere: Morse(o) Kargl(-)

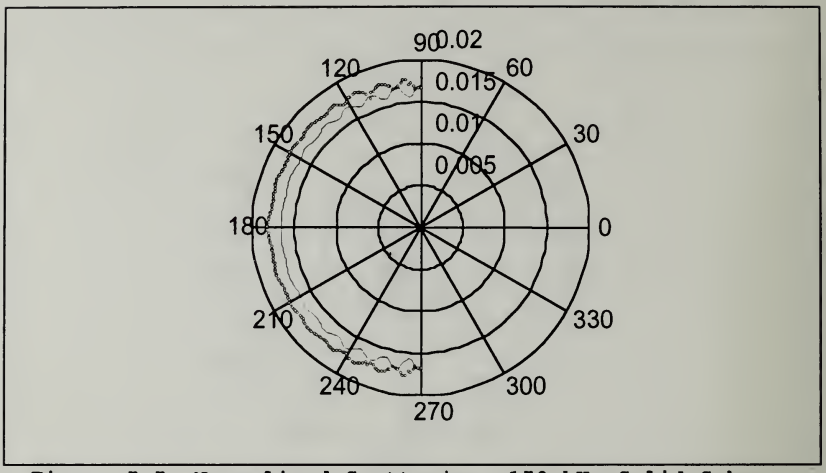

Figure 5.5. Normalized Scattering, 150 kHz Solid Sphere: Morse(dotted) and Kargl(solid)

C. COMPARISON OF EXPERIMENTAL RESULTS AND CALCULATIONS

Figures 5.6 through 5.15 show a comparison of the measured scattering with theoretical calculations for the 100 and the 500 micron spheres at five frequencies, 30, 60, 90, 120, and 150 kHz. The solid curve in each figure was generated by Kargl's program using the input data listed in Appendix C. The dashed curve is the scattering from a rigid and massive sphere following Morse. The open circles connected by dot-dash are data, where the dot-dash between the data points is simply a guide to the eye. It is obvious from the figures that the experimental and theoretical values do not agree for the input parameters used in the calculations.

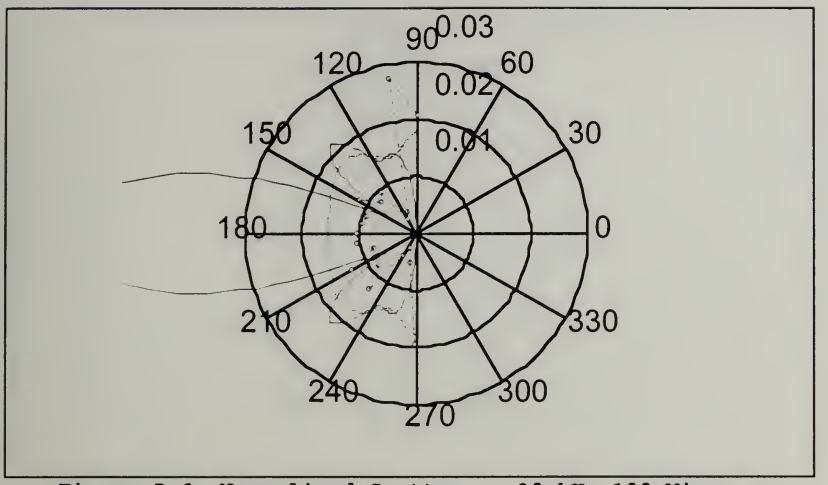

Figure 5.6. Normalized Scatterng, 30 kHz 100 Micron: Kargl(solid),Morse(dashed), & Exp. Data(dots superimposed)

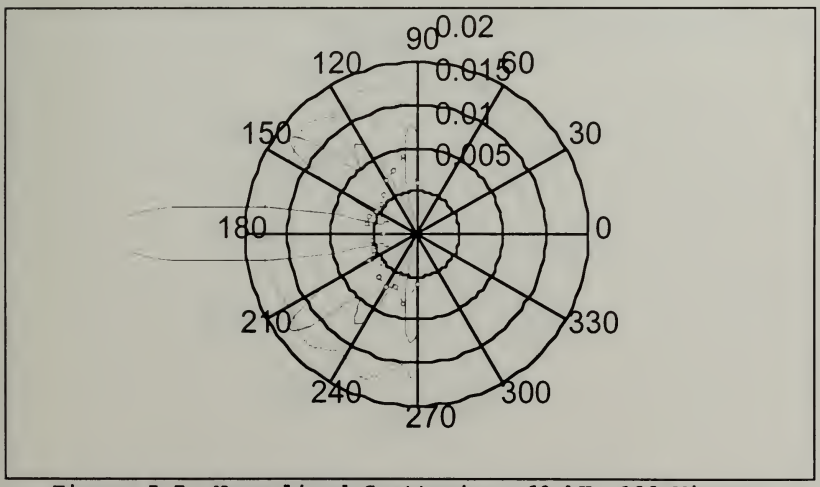

Figure 5.7. Normalized Scattering, 60 kHz 100 Micron: Kargl(solid), Morse(dashed), & Exp. Data(dots superimposed)

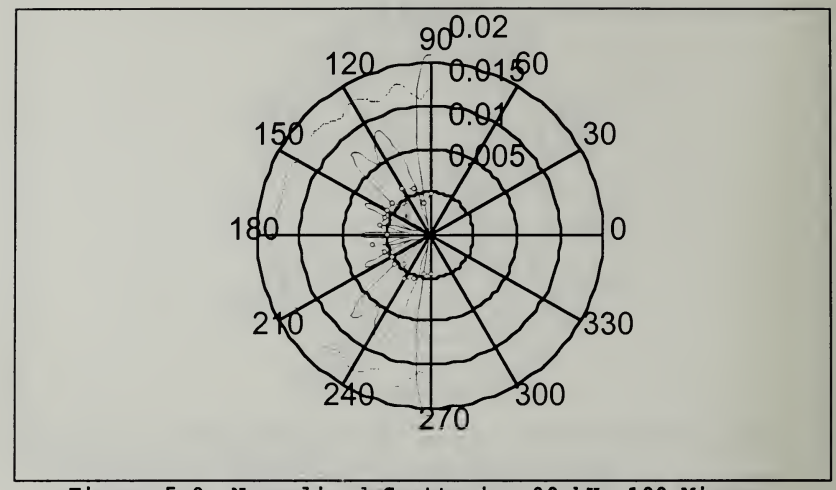

Figure 5.8. Normalized Scattering,90 kHz 100 Micron: Kargl(solid), Morse(dashed), & Exp. Data(dots superimposed)

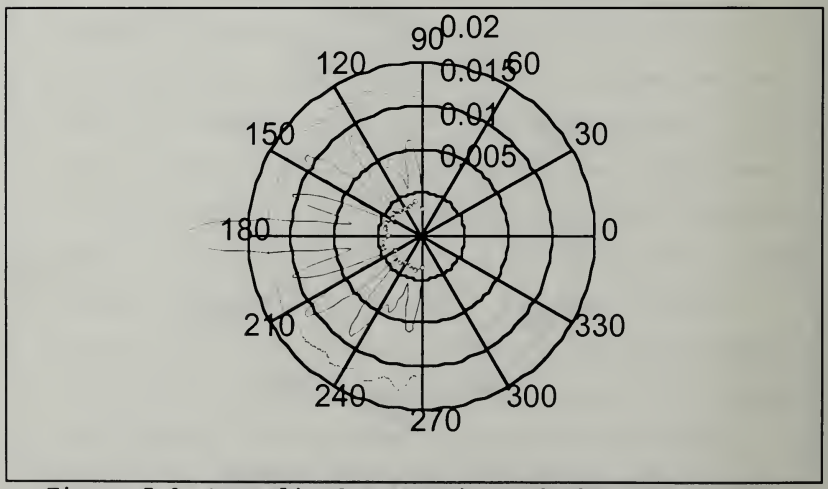

Figure 5.9. Normalized Scattering, 120 kHz 100 Micron: Kargl(solid),Morse(dashed), & Exp. Data(dots superimposed)

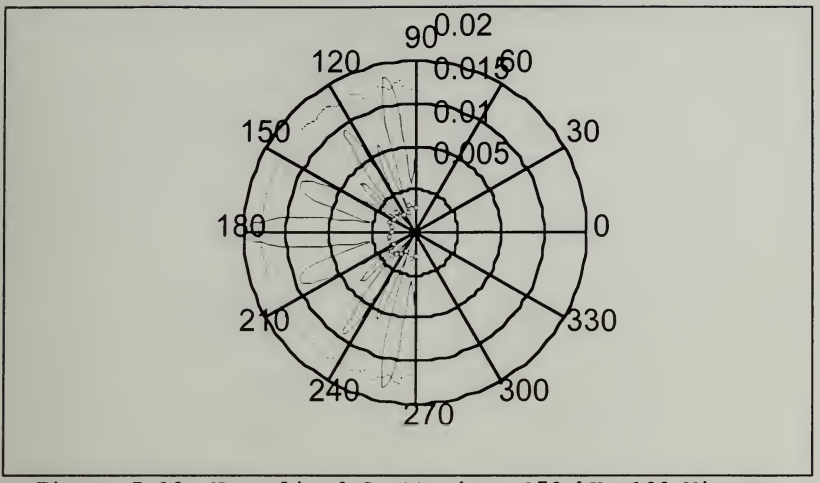

Figure 5.10. Normalized Scattering, 150 kHz 100 Micron: Kargl(solid), Morse(dashed), & Exp. Data(dots superimposed)

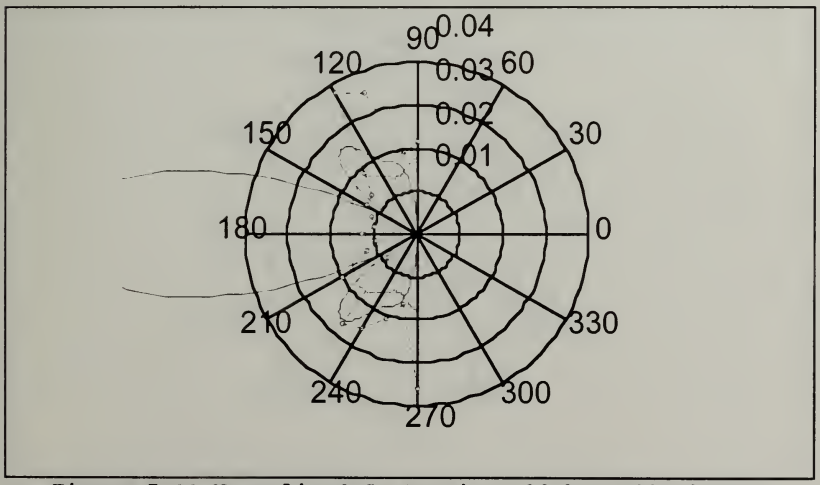

Figure 5.11 Normalized Scattering, 30 kHz 500 Micron: Kargl(solid), Morse(dashed),& Exp. Data(dotssuperimposed)

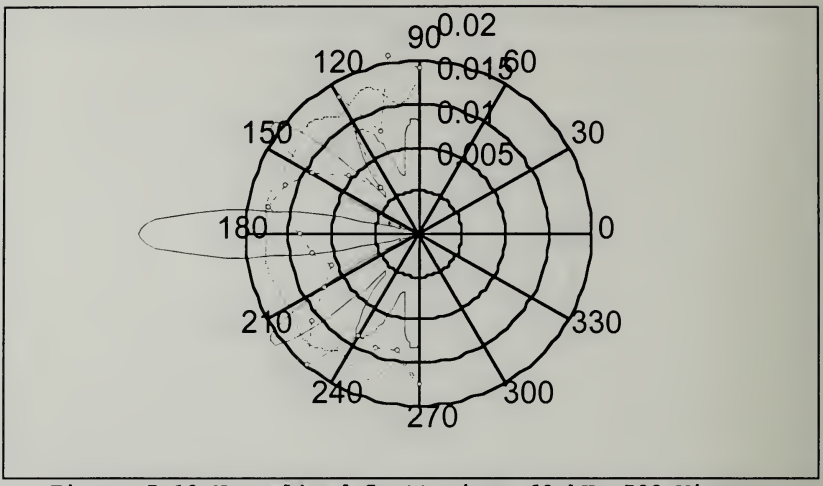

Figure 5.12 Normalized Scattering, 60 kHz 500 Micron: Kargl(solid), Morse(dashed), & Exp. Data(dots superimposed)

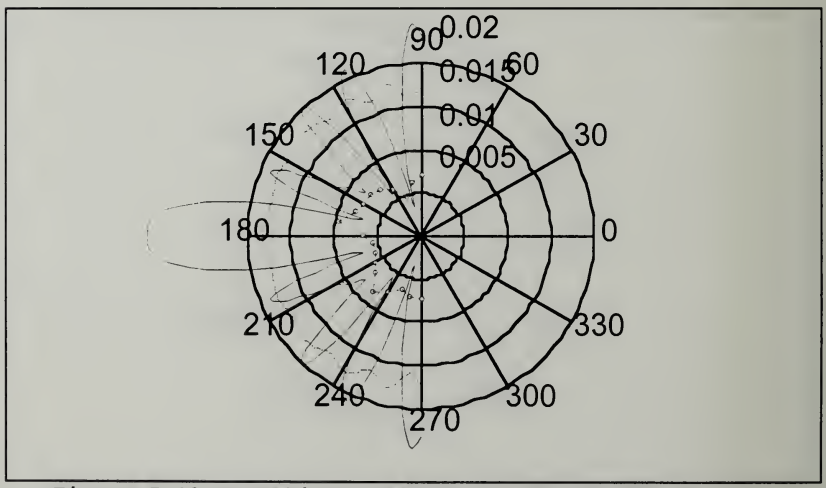

Figure 5.13 Normalized Scattering, 90 kHz 500 Micron: Kargl(solid), Morse(dashed), & Exp. Data(dots superimposed)

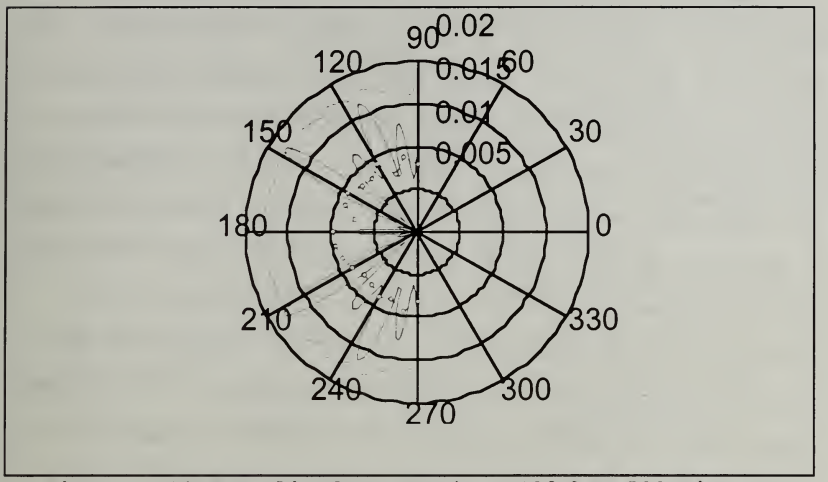

Figure 5.14 Normalized Scattering, 120 kHz 500 Micron: Kargl(solid), Morse(dashed), & Exp. Data(dots superimposed)

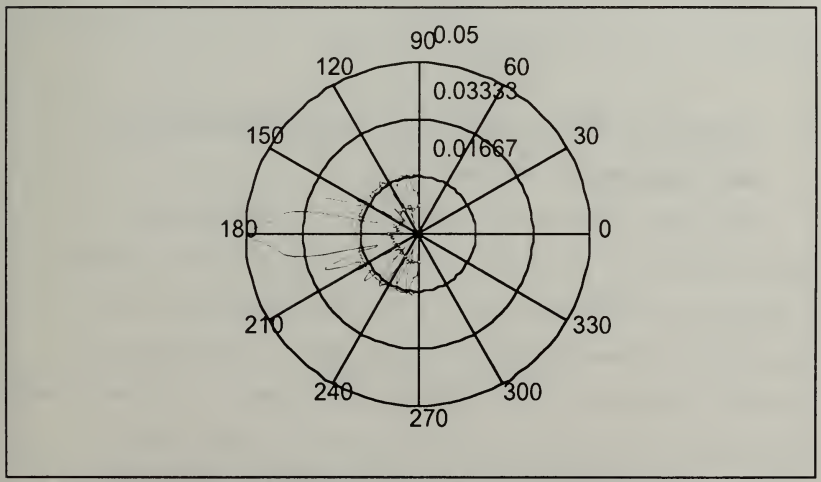

Figure 5.15 Normalized Scattering, 150 kHz 500 Micron: Kargl(solid), Morse(dashed), & Exp. Data(dots superimposed)

The most notable difference between the experimental and theoretical results are in (1) the overall amplitude of the scattering and (2) the structure in the angular dependence of the scattering. Generally, the observed scattering is much less than predicted. Regarding the angular dependence, the observed results resemble much more the scattering from a rigid and massive sphere with reduced amplitude, than the predicted results. It is not likely that the lack of structure in the observed scattering is a consequence of sampling the angular function every 10 degrees. In numerous cases there are several experimental samples within the angular ranges of a lobe in the predicted results. Furthermore, the 180 degree backscatter was measured at all frequencies, and no hint of strong lobing was experimentally observed in this direction.

D. SPECULATION FOR DISAGREEMENT BETWEEN THEORETICAL AND EXPERIMENTAL VALUES

The amplitude and structure of the calculated predictions for the scattering are suggestive of internal resonance in the scatter. It was speculated that the presence of these features may be due to the neglect of material damping of the porous solid frame in the calculated scattering. To test this speculation two additional calculations of scattering using Kargl's program were

performed. In the first case a damping value of 3% was used. This value was chosen based on Brown's measurement of the elastic modulus of a common epoxy (Brown, 1991, p. 41). The second test was performed using a damping value of 10%. This represent's a very large damping value. The values of the elastic moduli use in the calculations corresponding to these damping values are listed in Appendix C.

Figures 5.16 through 5.25 are comparisons between the theoretical values produced by Kargl's program with 3% damping (dashed curve), 10% damping (dotted curve), and experiment data (solid curve with dots superimposed).

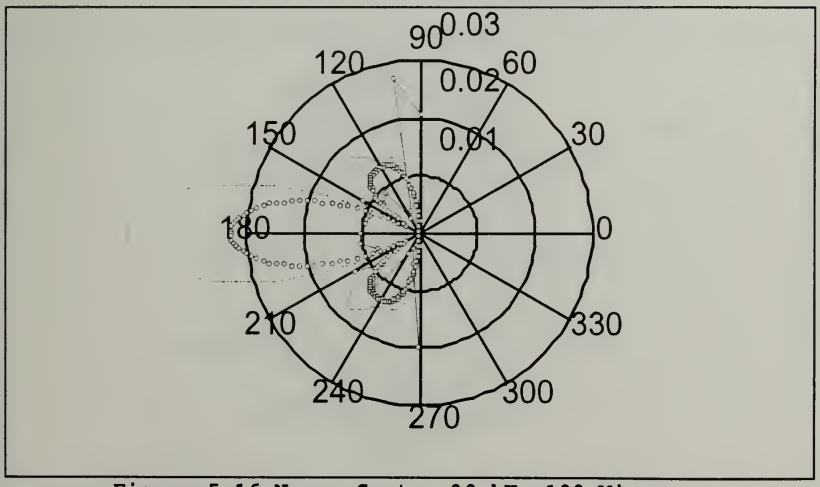

Figure 5.16 Norm. Scat., 30 kHz 100 Micron: 3% Damping(dashed), 10% Damping(dotted), & Experiment Data(dots superimposed)

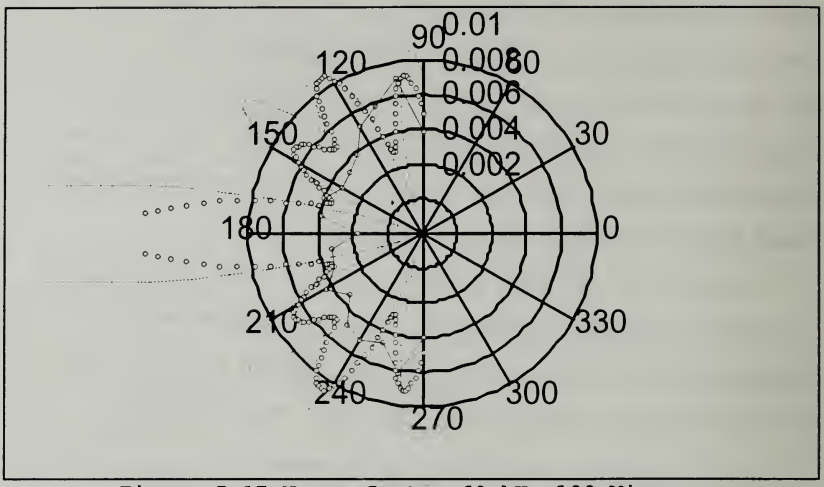

Figure 5.17 Norm. Scat., 60 kHz 100 Micron:
3% Damping(dashed), 10% Damping(dotted),
& Experiment Data(dots superimposed)

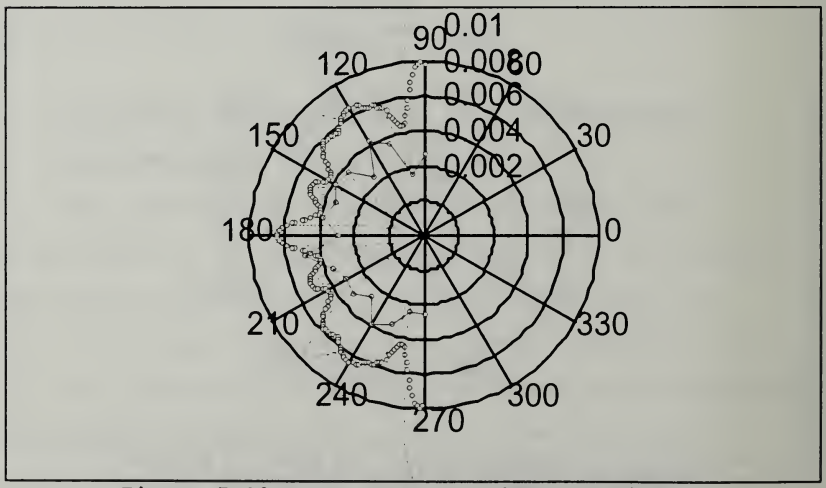

Figure 5.18 Norm. Scat., 90 kHz 100 Micron:
3% Damping(dashed), 10% Damping(dotted),
& Experiment Data(dots superimposed)

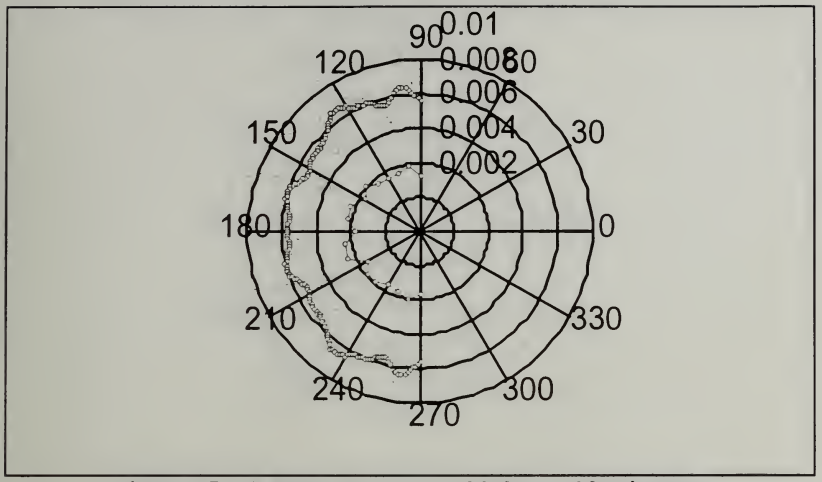

Figure 5.19 Norm. Scat., 120 kHz 100 Micron:
3% Damping(dashed), 10% Damping(dotted),
& Experiment Data(dots superimposed)

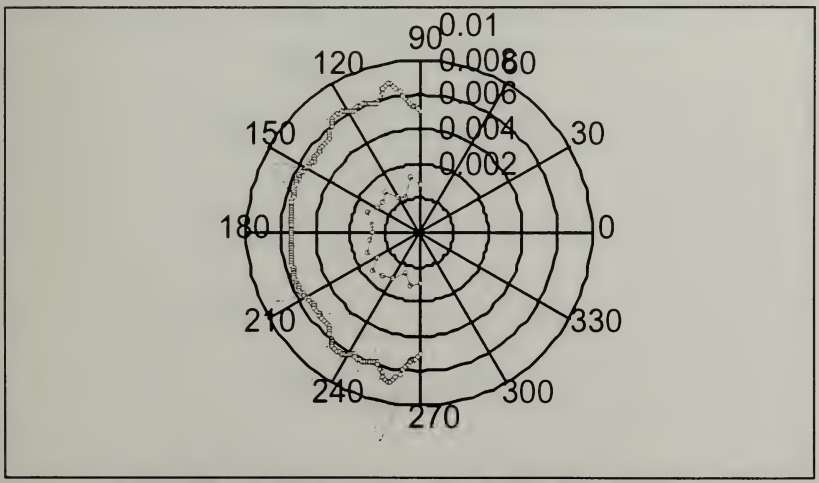

Figure 5.20 Norm. Scat., 150 kHz 100 Micron:
3% Damping(dashed), 10% Damping(dotted),
& Experiment Data(dots superimposed)

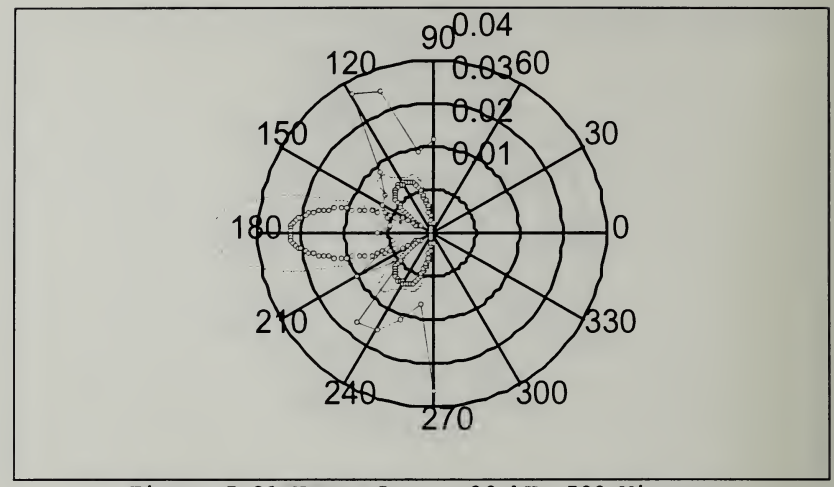

Figure 5.21 Norm. Scat., 30 kHz 500 Micron:
3% Damping(dashed), 10% Damping(dotted),
& Experiment Data(dots superimposed)

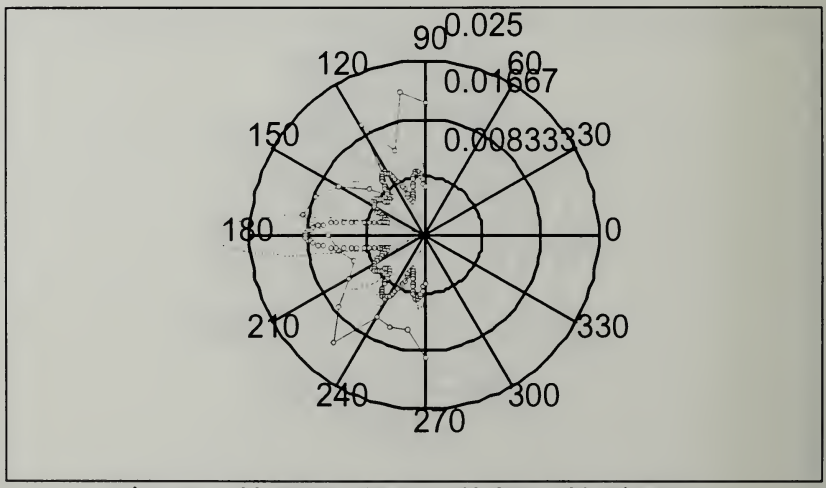

Figure 5.22 Norm. Scat., 60 kHz 500 Micron:
3% Damping(dashed), 10% Damping(dotted),
& Experiment Data(dots superimposed)

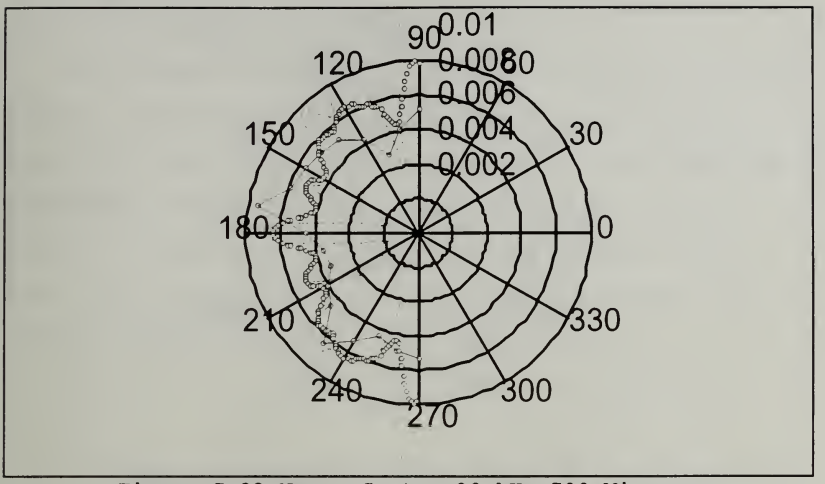

Figure 5.23 Norm. Scat., 90 kHz 500 Micron:
3% Damping(dashed), 10% Damping(dotted),
& Experiment Data(dots superimposed)

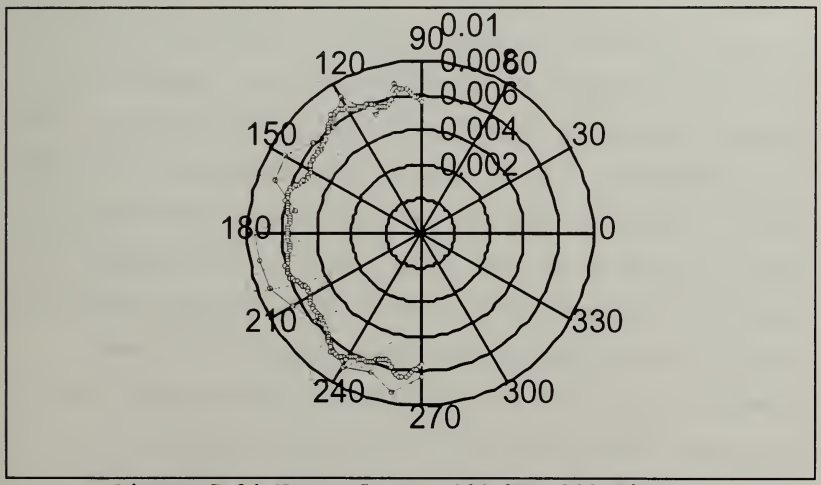

Figure 5.24 Norm. Scat., 120 kHz 500 Micron:
3% Damping(dshed), 10% Damping(dotted),
& Experiment Data(dots superimposed)

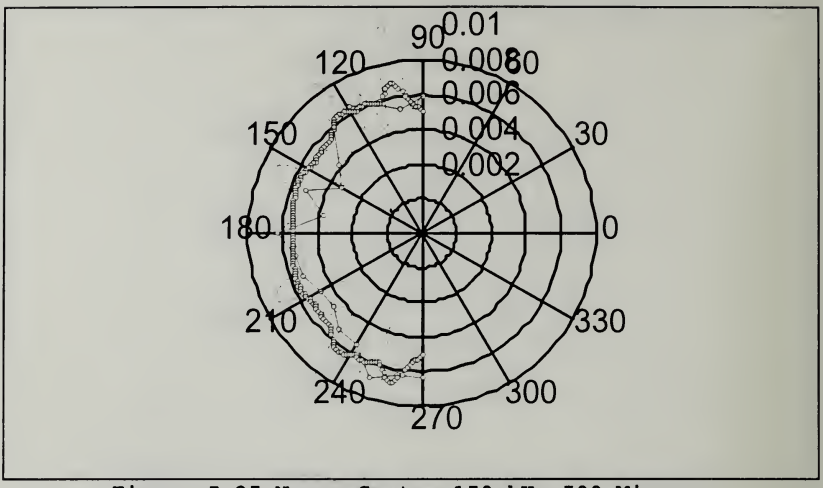

Figure 5.25 Norm. Scat., 150 kHz 500 Micron: 3% Damping(dashed), 10% Damping(dotted), & Experiment Data(dots superimposed)

From the figures it is apparent that including material damping in the skeletal frame substantially improves the agreement between measured and calculated scattering. Very close agreement is found between the experimental data and Kargl's curves for 10% damping for the 500 micron sample at frequencies of 90 kHz and above (Figures 5.23 through 5.25). Except for the pronounced lobe in the 180 degree backscatter direction predicted by the calculations, the agreement between the data and the 10% damping curves is fair for the 100 micron sample between 30 and 90 kHz (Figures 5.16 through 5.18). In the remaining cases the agreement is less

than good, with no recognizable trend with frequency or grain size (Figures 5.19 through 5.22).

As mentioned previously, a damping value of 10% is very large. It is a legitimate question as to whether this is realistic, even though the agreement between the data and 10% damping curves was better than for the 3% damping curves. As was mentioned previously, if greater aspect ratio (20:1) porous cylinder samples were available, the skeletal damping could be directly measured.

VI. SUMMARY, CONCLUSIONS, AND RECOMMENDATIONS

A. SUMMARY AND CONCLUSIONS

An experiment was performed to measure the scattering of underwater sound from a porous solid for the first time. Two porous solid spheres composed of heat-epoxied glass beads of 100 and 500 micron mean bead diameter were used. The permeability, porosity, and shear modulus of each sample were estimated from measurements made on cylindrical samples which had been manufactured at the same time and of the same glass beads as the spheres. These material properties were used as input to a theoretical model for the sound scattered from a poro-elastic sphere imbedded in a poro-elastic host developed by Kargl and Lim. The experimental data were compared to the theoretical calculations.

Theoretical calculations with 0%, 3%, and 10% skeletal frame damping were compared to experimental data. Very good agreement between measured and predicted scattering was obtained for each sample over certain frequency ranges, taking 10% frame damping in the calculations. For other frequency ranges the agreement was less than good. No systematic trend in the agreement could be discerned with regard to porous grain size or sound frequency.

B. RECOMMENDATIONS

Regarding the scattering, the greatest hinderance to obtaining better quality data was the small size of the tanks available at NPS. It is recommended that future measurements be conducted in a large tank. This would allow scattering measurements to be made down to lower frequencies, where the viscous drag on the fluid in the pores is more significant, and would also allow more of the angular dependence to be measured.

Regarding the calculation of the scattering, it is believed that all the material properties of the porous spheres are fairly well known except the sketal frame damping. Since it has a great influence on the scattering, it would be desirable to measure this directly. If greater aspect ratio (20:1) porous cylinder samples were available, both the torsional and longitudinal moduli and the damping coefficients could be measured.

Lastly, no attempt was made to measure the tortuosity of the present samples; a typical value was assumed based upon the porosity. Although it would not be expected to differ significantly, the tortuosity could be measured.

Appendix A: Experiment Data 100 Micron Sphere

090 Degrees					
Frequency	Scattered Voltage Peak	Incident Voltage Peak	Ratio of Scattered &	Radius	Normalized Voltage
150 K Hz	40.4383	6.4486	0.0063	0.4450	0.0028
140 K Hz	36.3745	5.6726	0.0064	0.4450	0.0029
130 K Hz	36.5558	5.3757	0.0068	0.4450	0.0030
120 K Hz	37.9287	5.2122	0.0073	0.4450	0.0032
110 K Hz	45.1342	4.8513	0.0093	0.4450	0.0041
100 K Hz	37.1727	3.6166	0.0103	0.4450	0.0046
90 K Hz	24.9800	2.3823	0.0105	0.4450	0.0047
80 K Hz	18.1007	1.5898	0.0114	0.4450	0.0051
70 K Hz	14.3538	1.2265	0.0117	0.4450	0.0052
60 K Hz	11.4788	0.8601	0.0133	0.4450	0.0059
50 K Hz	11.1717	0.5325	0.0210	0.4450	0.0093
40 K Hz	9.4783	0.3127	0.0303	0.4450	0.0135
30 K Hz	7.1300	0.1545	0.0461	0.4450	0.0205
100 Degrees					
150 K Hz	47.2183	6.4486	0.0073	0.4450	0.0033
140 K Hz	48.3593	5.6726	0.0085	0.4450	0.0038
130 K Hz	48.7275	5.3757	0.0091	0.4450	0.0040
120 K Hz	46.1983	5.2122	0.0089	0.4450	0.0039
110 K Hz	45.7013	4.8513	0.0094	0.4450	0.0042
100 K Hz	41.0225	3.6166	0.0113	0.4450	0.0050
90 K Hz	19.5000	2.3823	0.0082	0.4450	0.0036
80 K Hz	17.7602	1.5898	0.0112	0.4450	0.0050
70 K Hz	17.9715	1.2265	0.0147	0.4450	0.0065
60 K Hz	17.6110	0.8601	0.0205	0.4450	0.0091
50 K Hz	11.0512	0.5325	0.0208	0.4450	0.0092
40 K Hz	8.5500	0.3127	0.0273	0.4450	0.0122
30 K Hz	9.5092	0.1545	0.0615	0.4450	0.0274
110 Degrees					
150 K Hz	32.7883	6.4486	0.0051	0.4450	0.0023
140 K Hz	28.8460	5.6726	0.0051	0.4450	0.0023
130 K Hz	35.8323	5.3757	0.0067	0.4450	0.0030
120 K Hz	41.4358	5.2122	0.0079	0.4450	0.0035
110 K Hz	38.8262	4.8513	0.0080	0.4450	0.0036
100 K Hz	40.4590	3.6166	0.0112	0.4450	0.0050
90 K Hz	29.9790	2.3823	0.0126	0.4450	0.0056
80 K Hz	17.4180	1.5898	0.0110	0.4450	0.0049
70 K Hz	12.9720	1.2265	0.0106	0.4450	0.0047
60 K Hz	15.0676	0.8601	0.0175	0.4450	0.0078
50 K Hz	7.1738	0.5325	0.0135	0.4450	0.0060
40 K Hz	6.0420	0.3127	0.0193	0.4450	0.0086
30 K Hz	1.4373	0.1545	0.0093	0.4450	0.0041

Appendix A: Experimental Data 100 Micron Sphere

120 Degrees					
Frequency	Scattered Voltage Peak	Incident Voltage Peak	Ratio of Scattered &	Radius	Normalized Voltage
150 K Hz	34.8293	6.4486	0.0054	0.4450	0.0024
140 K Hz	37.9132	5.6726	0.0067	0.4450	0.0030
130 K Hz	35.8993	5.3757	0.0067	0.4450	0.0030
120 K Hz	41.5385	5.2122	0.0080	0.4450	0.0035
110 K Hz	45.2625	4.8513	0.0093	0.4450	0.0042
100 K Hz	44.4807	3.6166	0.0123	0.4450	0.0055
90 K Hz	33.2975	2.3823	0.0140	0.4450	0.0062
80 K Hz	17.2008	1.5898	0.0108	0.4450	0.0048
70 K Hz	16.5760	1.2265	0.0135	0.4450	0.0060
60 K Hz	13.7793	0.8601	0.0160	0.4450	0.0071
50 K Hz	4.5138	0.5325	0.0085	0.4450	0.0038
40 K Hz	3.9103	0.3127	0.0125	0.4450	0.0056
30 K Hz	1.0550	0.1545	0.0068	0.4450	0.0030
130 Degrees					
150 K Hz	45.0708	6.4486	0.0070	0.4450	0.0031
140 K Hz	39.5708	5.6726	0.0070	0.4450	0.0031
130 K Hz	39.4028	5.3757	0.0073	0.4450	0.0033
120 K Hz	43.7050	5.2122	0.0084	0.4450	0.0037
110 K Hz	52.1192	4.8513	0.0107	0.4450	0.0048
100 K Hz	43.6108	3.6166	0.0121	0.4450	0.0054
90 K Hz	23.3100	2.3823	0.0098	0.4450	0.0044
80 K Hz	22.6865	1.5898	0.0143	0.4450	0.0064
70 K Hz	12.7390	1.2265	0.0104	0.4450	0.0046
60 K Hz	11.4392	0.8601	0.0133	0.4450	0.0059
50 K Hz	5.5797	0.5325	0.0105	0.4450	0.0047
40 K Hz	5.4183	0.3127	0.0173	0.4450	0.0077
30 K Hz	3.2575	0.1545	0.0211	0.4450	0.0094
140 Degrees					
150 K Hz	40.3580	6.4486	0.0063	0.4450	0.0028
140 K Hz	40.1742	5.6726	0.0071	0.4450	0.0032
130 K Hz	37.7300	5.3757	0.0070	0.4450	0.0031
120 K Hz	48.4375	5.2122	0.0093	0.4450	0.0041
110 K Hz	44.6213	4.8513	0.0092	0.4450	0.0041
100 K Hz	45.3367	3.6166	0.0125	0.4450	0.0056
90 K Hz	30.2810	2.3823	0.0127	0.4450	0.0057
80 K Hz	22.4520	1.5898	0.0141	0.4450	0.0063
70 K Hz	15.0342	1.2265	0.0123	0.4450	0.0055
60 K Hz	10.5680	0.8601	0.0123	0.4450	0.0055
50 K Hz	7.0125	0.5325	0.0132	0.4450	0.0059
40 K Hz	5.4743	0.3127	0.0175	0.4450	0.0078
30 K Hz	2.8742	0.1545	0.0186	0.4450	0.0083

Appendix A: Experimental Data 100 Micron Sphere

150 Degrees					
Frequency	Scattered Voltage Peak	Incident Voltage Peak	Ratio of Scattered &	Radius	Normalized Voltage
150 K Hz	41.4772	6.4486	0.0064	0.4450	0.0029
140 K Hz	38.5983	5.6726	0.0068	0.4450	0.0030
130 K Hz	37.9283	5.3757	0.0071	0.4450	0.0031
120 K Hz	43.2050	5.2122	0.0083	0.4450	0.0037
110 K Hz	44.0067	4.8513	0.0091	0.4450	0.0040
100 K Hz	39.0245	3.6166	0.0108	0.4450	0.0048
90 K Hz	31.3458	2.3823	0.0132	0.4450	0.0059
80 K Hz	16.0492	1.5898	0.0101	0.4450	0.0045
70 K Hz	16.3790	1.2265	0.0134	0.4450	0.0059
60 K Hz	10.2267	0.8601	0.0119	0.4450	0.0053
50 K Hz	8.3867	0.5325	0.0157	0.4450	0.0070
40 K Hz	5.5633	0.3127	0.0178	0.4450	0.0079
30 K Hz	4.0188	0.1545	0.0260	0.4450	0.0116
160 Degrees					
150 K Hz	47.1867	6.4486	0.0073	0.4450	0.0033
140 K Hz	35.3850	5.6726	0.0062	0.4450	0.0028
130 K Hz	44.5260	5.3757	0.0083	0.4450	0.0037
120 K Hz	50.2040	5.2122	0.0096	0.4450	0.0043
110 K Hz	51.1700	4.8513	0.0105	0.4450	0.0047
100 K Hz	33.9697	3.6166	0.0094	0.4450	0.0042
90 K Hz	29.2012	2.3823	0.0123	0.4450	0.0055
80 K Hz	20.0092	1.5898	0.0126	0.4450	0.0056
70 K Hz	16.2833	1.2265	0.0133	0.4450	0.0059
60 K Hz	11.5121	0.8601	0.0134	0.4450	0.0060
50 K Hz	7.1388	0.5325	0.0134	0.4450	0.0060
40 K Hz	5.8792	0.3127	0.0188	0.4450	0.0084
30 K Hz	3.1567	0.1545	0.0204	0.4450	0.0091
170 Degrees					
150 K Hz	39.1083	6.4486	0.0061	0.4450	0.0027
140 K Hz	33.7808	5.6726	0.0060	0.4450	0.0027
130 K Hz	42.8598	5.3757	0.0080	0.4450	0.0035
120 K Hz	50.0983	5.2122	0.0096	0.4450	0.0043
110 K Hz	53.5242	4.8513	0.0110	0.4450	0.0049
100 K Hz	43.6250	3.6166	0.0121	0.4450	0.0054
90 K Hz	31.3225	2.3823	0.0131	0.4450	0.0059
80 K Hz	18.3778	1.5898	0.0116	0.4450	0.0051
70 K Hz	17.6983	1.2265	0.0144	0.4450	0.0064
60 K Hz	11.4696	0.8601	0.0133	0.4450	0.0059
50 K Hz	10.5300	0.5325	0.0198	0.4450	0.0088
40 K Hz	5.4933	0.3127	0.0176	0.4450	0.0078
30 K Hz	3.3667	0.1545	0.0218	0.4450	0.0097

Appendix A: Experiment Data 100 Micron Sphere

180 Degrees					
Frequency	Scattered Voltage Peak	Incident Voltage Peak	Ratio of Scattered &	Radius	Normalized Voltage
150 K Hz	38.3327	6.4486	0.0059	0.4450	0.0026
140 K Hz	40.4618	5.6726	0.0071	0.4450	0.0032
130 K Hz	40.0060	5.3757	0.0074	0.4450	0.0033
120 K Hz	43.5560	5.2122	0.0084	0.4450	0.0037
110 K Hz	41.9475	4.8513	0.0086	0.4450	0.0038
100 K Hz	36.8025	3.6166	0.0102	0.4450	0.0045
90 K Hz	26.1592	2.3823	0.0110	0.4450	0.0049
80 K Hz	17.8428	1.5898	0.0112	0.4450	0.0050
70 K Hz	16.6760	1.2265	0.0136	0.4450	0.0061
60 K Hz	7.3292	0.8601	0.0085	0.4450	0.0038
50 K Hz	8.7313	0.5325	0.0164	0.4450	0.0073
40 K Hz	5.4558	0.3127	0.0174	0.4450	0.0078
30 K Hz	3.5700	0.1545	0.0231	0.4450	0.0103
190 Degrees					
150 K Hz	42.2913	6.4486	0.0066	0.4450	0.0029
140 K Hz	43.3332	5.6726	0.0076	0.4450	0.0034
130 K Hz	43.1792	5.3757	0.0080	0.4450	0.0036
120 K Hz	51.4793	5.2122	0.0099	0.4450	0.0044
110 K Hz	57.0342	4.8513	0.0118	0.4450	0.0052
100 K Hz	48.0690	3.6166	0.0133	0.4450	0.0059
90 K Hz	36.7250	2.3823	0.0154	0.4450	0.0069
80 K Hz	22.3860	1.5898	0.0141	0.4450	0.0063
70 K Hz	20.1035	1.2265	0.0164	0.4450	0.0073
60 K Hz	10.3447	0.8601	0.0120	0.4450	0.0054
50 K Hz	9.9688	0.5325	0.0187	0.4450	0.0083
40 K Hz	6.4400	0.3127	0.0206	0.4450	0.0092
30 K Hz	3.6900	0.1545	0.0239	0.4450	0.0106
200 Degrees					
150 K Hz	47.0758	6.4486	0.0073	0.4450	0.0032
140 K Hz	44.2468	5.6726	0.0078	0.4450	0.0035
130 K Hz	48.8900	5.3757	0.0091	0.4450	0.0040
120 K Hz	52.9118	5.2122	0.0102	0.4450	0.0045
110 K Hz	55.8542	4.8513	0.0115	0.4450	0.0051
100 K Hz	41.5592	3.6166	0.0115	0.4450	0.0051
90 K Hz	29.8485	2.3823	0.0125	0.4450	0.0056
80 K Hz	21.7983	1.5898	0.0137	0.4450	0.0061
70 K Hz	18.9125	1.2265	0.0154	0.4450	0.0069
60 K Hz	10.3852	0.8601	0.0121	0.4450	0.0054
50 K Hz	6.4110	0.5325	0.0120	0.4450	0.0054
40 K Hz	4.6800	0.3127	0.0150	0.4450	0.0067
30 K Hz	2.7383	0.1545	0.0177	0.4450	0.0079

Appendix A: Experiment Data 100 Micron Sphere

210 Degrees					
Frequency	Scattered Voltage Peak	Incident Voltage Peak	Ratio of Scattered &	Radius	Normalized Voltage
150 K Hz	41.4642	6.4486	0.0064	0.4450	0.0029
140 K Hz	38.0506	5.6726	0.0067	0.4450	0.0030
130 K Hz	40.8980	5.3757	0.0076	0.4450	0.0034
120 K Hz	41.1975	5.2122	0.0079	0.4450	0.0035
110 K Hz	43.7592	4.8513	0.0090	0.4450	0.0040
100 K Hz	36.2105	3.6166	0.0100	0.4450	0.0045
90 K Hz	27.4817	2.3823	0.0115	0.4450	0.0051
80 K Hz	15.0542	1.5898	0.0095	0.4450	0.0042
70 K Hz	16.3265	1.2265	0.0133	0.4450	0.0059
60 K Hz	12.3025	0.8601	0.0143	0.4450	0.0064
50 K Hz	6.6985	0.5325	0.0126	0.4450	0.0056
40 K Hz	5.0305	0.3127	0.0161	0.4450	0.0072
30 K Hz	4.5123	0.1545	0.0292	0.4450	0.0130
220 Degrees					
150 K Hz	51.0585	6.4486	0.0079	0.4450	0.0035
140 K Hz	40.1850	5.6726	0.0071	0.4450	0.0032
130 K Hz	41.7008	5.3757	0.0078	0.4450	0.0035
120 K Hz	46.0308	5.2122	0.0088	0.4450	0.0039
110 K Hz	43.2117	4.8513	0.0089	0.4450	0.0040
100 K Hz	39.1815	3.6166	0.0108	0.4450	0.0048
90 K Hz	28.3012	2.3823	0.0119	0.4450	0.0053
80 K Hz	20.2500	1.5898	0.0127	0.4450	0.0057
70 K Hz	15.7343	1.2265	0.0128	0.4450	0.0057
60 K Hz	10.5950	0.8601	0.0123	0.4450	0.0055
50 K Hz	9.7442	0.5325	0.0183	0.4450	0.0081
40 K Hz	5.2073	0.3127	0.0167	0.4450	0.0074
30 K Hz	2.9100	0.1545	0.0188	0.4450	0.0084
230 Degrees					
150 K Hz	48.0640	6.4486	0.0075	0.4450	0.0033
140 K Hz	46.9388	5.6726	0.0083	0.4450	0.0037
130 K Hz	46.5668	5.3757	0.0087	0.4450	0.0039
120 K Hz	45.9520	5.2122	0.0088	0.4450	0.0039
110 K Hz	51.6873	4.8513	0.0107	0.4450	0.0047
100 K Hz	44.0717	3.6166	0.0122	0.4450	0.0054
90 K Hz	24.6405	2.3823	0.0103	0.4450	0.0046
80 K Hz	23.4095	1.5898	0.0147	0.4450	0.0066
70 K Hz	14.2932	1.2265	0.0117	0.4450	0.0052
60 K Hz	13.1686	0.8601	0.0153	0.4450	0.0068
50 K Hz	6.8190	0.5325	0.0128	0.4450	0.0057
40 K Hz	5.8380	0.3127	0.0187	0.4450	0.0083
30 K Hz	4.4325	0.1545	0.0287	0.4450	0.0128

Appendix A: Experiment Data 100 Micron Sphere

240 Degrees					
Frequency	Scattered Voltage Peak	Incident Voltage Peak	Ratio of Scattered &	Radius	Normalized Voltage
150 K Hz	44.7043	6.4486	0.0069	0.4450	0.0031
140 K Hz	37.9132	5.6726	0.0067	0.4450	0.0030
130 K Hz	41.4555	5.3757	0.0077	0.4450	0.0034
120 K Hz	41.5002	5.2122	0.0080	0.4450	0.0035
110 K Hz	46.9225	4.8513	0.0097	0.4450	0.0043
100 K Hz	41.5600	3.6166	0.0115	0.4450	0.0051
90 K Hz	31.5850	2.3823	0.0133	0.4450	0.0059
80 K Hz	14.4007	1.5898	0.0091	0.4450	0.0040
70 K Hz	16.7046	1.2265	0.0136	0.4450	0.0061
60 K Hz	13.7793	0.8601	0.0160	0.4450	0.0071
50 K Hz	5.9080	0.5325	0.0111	0.4450	0.0049
40 K Hz	3.6175	0.3127	0.0116	0.4450	0.0051
30 K Hz	1.4740	0.1545	0.0095	0.4450	0.0042
250 Degrees					
150 K Hz	36.7973	6.4486	0.0057	0.4450	0.0025
140 K Hz	32.2718	5.6726	0.0057	0.4450	0.0025
130 K Hz	39.6038	5.3757	0.0074	0.4450	0.0033
120 K Hz	43.9790	5.2122	0.0084	0.4450	0.0038
110 K Hz	41.8430	4.8513	0.0086	0.4450	0.0038
100 K Hz	39.3550	3.6166	0.0109	0.4450	0.0048
90 K Hz	29.6080	2.3823	0.0124	0.4450	0.0055
80 K Hz	15.4360	1.5898	0.0097	0.4450	0.0043
70 K Hz	11.0180	1.2265	0.0090	0.4450	0.0040
60 K Hz	12.9610	0.8601	0.0151	0.4450	0.0067
50 K Hz	7.0217	0.5325	0.0132	0.4450	0.0059
40 K Hz	5.2700	0.3127	0.0169	0.4450	0.0075
30 K Hz	0.9785	0.1545	0.0063	0.4450	0.0028
260 Degrees					
150 K Hz	46.0317	6.4486	0.0071	0.4450	0.0032
140 K Hz	48.6158	5.6726	0.0086	0.4450	0.0038
130 K Hz	47.9885	5.3757	0.0089	0.4450	0.0040
120 K Hz	46.9222	5.2122	0.0090	0.4450	0.0040
110 K Hz	42.4220	4.8513	0.0087	0.4450	0.0039
100 K Hz	41.3200	3.6166	0.0114	0.4450	0.0051
90 K Hz	23.8667	2.3823	0.0100	0.4450	0.0045
80 K Hz	14.5722	1.5898	0.0092	0.4450	0.0041
70 K Hz	14.6733	1.2265	0.0120	0.4450	0.0053
60 K Hz	15.8470	0.8601	0.0184	0.4450	0.0082
50 K Hz	9.9700	0.5325	0.0187	0.4450	0.0083
40 K Hz	6.4500	0.3127	0.0206	0.4450	0.0092
30 K Hz	1.8105	0.1545	0.0117	0.4450	0.0052

Appendix A: Experiment Data 100 Micron Sphere

270 Degrees					
Frequency	Scattered Voltage Peak	Incident Voltage Peak	Ratio of Scattered &	Radius	Normalized Voltage
150 K Hz	42.8842	6.4486	0.0067	0.4450	0.0030
140 K Hz	41.1298	5.6726	0.0073	0.4450	0.0032
130 K Hz	39.1200	5.3757	0.0073	0.4450	0.0032
120 K Hz	42.4388	5.2122	0.0081	0.4450	0.0036
110 K Hz	43.6107	4.8513	0.0090	0.4450	0.0040
100 K Hz	36.7892	3.6166	0.0102	0.4450	0.0045
90 K Hz	24.2958	2.3823	0.0102	0.4450	0.0045
80 K Hz	21.5150	1.5898	0.0135	0.4450	0.0060
70 K Hz	18.6138	1.2265	0.0152	0.4450	0.0068
60 K Hz	11.6650	0.8601	0.0136	0.4450	0.0060
50 K Hz	8.7938	0.5325	0.0165	0.4450	0.0073
40 K Hz	6.8925	0.3127	0.0220	0.4450	0.0098
30 K Hz	6.8300	0.1545	0.0442	0.4450	0.0197

Appendix B: Experiment Data 500 Micron Sphere

90 Degrees					
Frequency	Scattered Voltage Peak	Incident Voltage Peak	Ratio of Scattered &	Radius	Normalized Voltage
150 K Hz	95.3333	5.3727	0.0177	0.4500	0.0080
120 K Hz	72.9500	4.2008	0.0174	0.4500	0.0078
90 K Hz	34.8250	2.1966	0.0159	0.4500	0.0071
60 K Hz	16.3583	0.3847	0.0425	0.4500	0.0191
30 K Hz	7.4350	0.1543	0.0482	0.4500	0.0217
100 Degrees					
150 K Hz	84.5083	5.3727	0.0157	0.4600	0.0072
120 K Hz	80.5583	4.2008	0.0192	0.4600	0.0088
90 K Hz	29.5333	2.1966	0.0134	0.4600	0.0062
60 K Hz	17.5533	0.3847	0.0456	0.4600	0.0210
30 K Hz	6.3375	0.1543	0.0411	0.4600	0.0189
110 Degrees					
150 K Hz	94.4000	5.3727	0.0176	0.4530	0.0080
120 K Hz	68.0333	4.2008	0.0162	0.4530	0.0073
90 K Hz	23.1333	2.1966	0.0105	0.4530	0.0048
60 K Hz	10.8000	0.3847	0.0281	0.4530	0.0127
30 K Hz	11.9300	0.1543	0.0773	0.4530	0.0350
120 Degrees					
150 K Hz	99.7667	5.3727	0.0186	0.4550	0.0084
120 K Hz	84.4750	4.2008	0.0201	0.4550	0.0091
90 K Hz	30.3500	2.1966	0.0138	0.4550	0.0063
60 K Hz	15.2967	0.3847	0.0398	0.4550	0.0181
30 K Hz	12.7250	0.1543	0.0825	0.4550	0.0375
130 Degrees					
150 K Hz	92.0750	5.3727	0.0171	0.4550	0.0078
120 K Hz	73.5083	4.2008	0.0175	0.4550	0.0080
90 K Hz	34.4450	2.1966	0.0157	0.4550	0.0071
60 K Hz	5.9200	0.3847	0.0154	0.4550	0.0070
30 K Hz	6.2733	0.1543	0.0406	0.4550	0.0185
140 Degrees					
150 K Hz	72.3700	5.3727	0.0135	0.4570	0.0062
120 K Hz	75.6083	4.2008	0.0180	0.4570	0.0082
90 K Hz	35.5358	2.1966	0.0162	0.4570	0.0074
60 K Hz	8.7117	0.3847	0.0226	0.4570	0.0103
30 K Hz	4.6833	0.1543	0.0303	0.4570	0.0139

Appendix B: Experiment Data 500 Micron Sphere

150 Degrees					
Frequency	Scattered Voltage Peak	Incident Voltage Peak	Ratio of Scattered &	Radius	Normalized Voltage
150 K Hz	62.8250	5.3727	0.0117	0.4520	0.0053
120 K Hz	84.8000	4.2008	0.0202	0.4520	0.0091
90 K Hz	36.4333	2.1966	0.0166	0.4520	0.0075
60 K Hz	12.1000	0.3847	0.0315	0.4520	0.0142
30 K Hz	4.5417	0.1543	0.0294	0.4520	0.0133
160 Degrees					
150 K Hz	85.3250	5.3727	0.0159	0.4500	0.0071
120 K Hz	83.9083	4.2008	0.0200	0.4500	0.0090
90 K Hz	38.3750	2.1966	0.0175	0.4500	0.0079
60 K Hz	14.0833	0.3847	0.0366	0.4500	0.0165
30 K Hz	3.8133	0.1543	0.0247	0.4500	0.0111
170 Degrees					
150 K Hz	67.6250	5.3727	0.0126	0.4550	0.0057
120 K Hz	67.6000	4.2008	0.0161	0.4550	0.0073
90 K Hz	45.9917	2.1966	0.0209	0.4550	0.0095
60 K Hz	14.9250	0.3847	0.0388	0.4550	0.0177
30 K Hz	3.3950	0.1543	0.0220	0.4550	0.0100
180 Degrees					
150 K Hz	100.8000	5.3727	0.0188	0.4450	0.0083
120 K Hz	90.9667	4.2008	0.0217	0.4450	0.0096
90 K Hz	32.5583	2.1966	0.0148	0.4450	0.0066
60 K Hz	11.7917	0.3847	0.0307	0.4450	0.0136
30 K Hz	4.3500	0.1543	0.0282	0.4450	0.0125
190 Degrees					
150 K Hz	89.5250	5.3727	0.0167	0.4430	0.0074
120 K Hz	89.9917	4.2008	0.0214	0.4430	0.0095
90 K Hz	27.8833	2.1966	0.0127	0.4430	0.0056
60 K Hz	10.7333	0.3847	0.0279	0.4430	0.0124
30 K Hz	3.2400	0.1543	0.0210	0.4430	0.0093
200 Degrees					
150 K Hz	86.8833	5.3727	0.0162	0.4450	0.0072
120 K Hz	87.7417	4.2008	0.0209	0.4450	0.0093
90 K Hz	26.7333	2.1966	0.0122	0.4450	0.0054
60 K Hz	9.2375	0.3847	0.0240	0.4450	0.0107
30 K Hz	4.2133	0.1543	0.0273	0.4450	0.0121

Appendix B: Experiment Data 500 Micron Sphere

210 Degrees					
Frequency	Scattered Voltage Peak	Incident Voltage Peak	Ratio of Scattered &	Radius	Normalized Voltage
150 K Hz	81.8753	5.3727	0.0152	0.4430	0.0068
120 K Hz	80.9833	4.2008	0.0193	0.4430	0.0085
90 K Hz	30.1917	2.1966	0.0137	0.4430	0.0061
60 K Hz	10.8608	0.3847	0.0282	0.4430	0.0125
30 K Hz	6.9017	0.1543	0.0447	0.4430	0.0198
220 Degrees					
150 K Hz	79.8800	5.3727	0.0149	0.4450	0.0066
120 K Hz	75.3417	4.2008	0.0179	0.4450	0.0080
90 K Hz	33.0000	2.1966	0.0150	0.4450	0.0067
60 K Hz	13.8337	0.3847	0.0360	0.4450	0.0160
30 K Hz	3.0500	0.1543	0.0198	0.4450	0.0088
230 Degrees					
150 K Hz	88.4917	5.3727	0.0165	0.4450	0.0073
120 K Hz	76.9917	4.2008	0.0183	0.4450	0.0082
90 K Hz	42.0100	2.1966	0.0191	0.4450	0.0085
60 K Hz	17.2583	0.3847	0.0449	0.4450	0.0200
30 K Hz	9.3983	0.1543	0.0609	0.4450	0.0271
240 Degrees					
150 K Hz	89.5167	5.3727	0.0167	0.4490	0.0075
120 K Hz	83.4667	4.2008	0.0199	0.4490	0.0089
90 K Hz	36.0033	2.1966	0.0164	0.4490	0.0074
60 K Hz	11.7692	0.3847	0.0306	0.4490	0.0137
30 K Hz	8.8000	0.1543	0.0570	0.4490	0.0256
250 Degrees					
150 K Hz	105.2917	5.3727	0.0196	0.4540	0.0089
120 K Hz	79.0583	4.2008	0.0188	0.4540	0.0085
90 K Hz	31.3250	2.1966	0.0143	0.4540	0.0065
60 K Hz	11.9083	0.3847	0.0310	0.4540	0.0141
30 K Hz	7.1800	0.1543	0.0465	0.4540	0.0211
260 Degrees					
150 K Hz	98.1417	5.3727	0.0183	0.4540	0.0083
120 K Hz	86.1750	4.2008	0.0205	0.4540	0.0093
90 K Hz	34.1500	2.1966	0.0155	0.4540	0.0071
60 K Hz	11.5633	0.3847	0.0301	0.4540	0.0136
30 K Hz	5.6000	0.1543	0.0363	0.4540	0.0165

Appendix B: Experiment Data 500 Micron Sphere

270 Degrees					
Frequency	Scattered Voltage Peak	Incident Voltage Peak	Ratio of Scattered &	Radius	Normalized Voltage
150 K Hz	96.2083	5.3727	0.0179	0.4700	0.0084
120 K Hz	74.1000	4.2008	0.0176	0.4700	0.0083
90 K Hz	33.9167	2.1966	0.0154	0.4700	0.0073
60 K Hz	14.3000	0.3847	0.0372	0.4700	0.0175
30 K Hz	11.8750	0.1543	0.0769	0.4700	0.0362

Appendix C
Input to Kargl's Program: 100 Micron Case

Parameter	Name	0% Damping	3% Damping	10% Damping
Host (Water)				
density, ρ	rho	1000	1000	1000
Bulk Modulus, K	ks	2.25×10^{9}	2.25×10^{9}	2.25×10^{9}
Shear Modulus, N	emu	0.0	0.0	0.0
porosity, P	beta	0.99999	0.99999	0.99999
permeability, k	kd	1.0	1.0	1.0
min wave number	x1min	0	0	0
max wave number	x1max	50	50	50
Porous Sphere				
radius	radius	0.332	0.332	0.332
density, ρ Bulk	rho0	2231	2231	2231
Bulk Modulus, K	ks0	3.5×10^{10}	3.5×10^{10}	3.5×10^{10}
Shear Modulus, N	emu0	2.6×10^{-10}	2.6×10^{-10}	2.6×10^{-10}
porosity, P	beta0	0.31	0.31	0.31
permeability, k	kd0	6.5×10^{-12}	6.5×10^{-12}	6.5×10^{-12}
Exterior Fluid				
density, ρ	rhof	1000	1000	1000
Bulk Modul, K	kf	2.25×10^{9}	2.25×10^{9}	2.25×10^{9}
viscosity, η	eta	0.0	0.0	0.0
Internal Fluid				
density, ρ	rhof0	1000	1000	1000
Bulk Modulus, K	kf0	2.25×10^{9}	2.25×10^{9}	2.25×10^{9}
viscosity, η	eta0	0.001	0.001	0.001
Others				
	dist	0.45	0.45	0.45
	hash	1	1	1
	nstart	0	0	0
	nend	75	75	75
	exp	1	1	1
	exp0	1	1	1
	nangle	361	361	361
	nfreq	5	5	5
	freqmin	30,000	30,000	30,000
	dfreq	30,000	30,000	30,000

Appendix C
Input Data for Kargl's Program: 500 Micron

Parameter	Name	0% Damping	3% Damping	10% Damping
Host (Water)				
density, ρ	rho	1000	1000	1000
Bulk Modulus, K	ks	2.25×10^{9}	2.25×10^{9}	2.25×10^{9}
Shear Modulus, N	emu	0.0	0.0	0.0
porosity, P	beta	0,99999	0.99999	0.99999
permeability, k	kd	1.0	1.0	1.0
min wave number	x1min	0	0	0
max wave number	x1max	50	50	50
Porous Sphere				
radius	radius	0.332	0.332	0.332
density, ρ Bulk	rho0	2231	2231	2231
Bulk Modulus, K	ks0	3.5×10^{10}	3.5×10^{10}	3.5×10^{10}
Shear Modulus, N	emu0	2.6×10^{-10}	2.6×10^{-10}	2.6×10^{-10}
porosity, P	beta0	0.32	0.32	0.32
permeability, k	kd0	5.74×10^{-11}	5.74×10^{-11}	5.74×10^{-11}
Exterior Fluid				
density, ρ	rhof	1000	1000	1000
Bulk Modul, K	kf	2.25×10^{9}	2.25×10^{9}	2.25×10^{9}
viscosity, η	eta	0.0	0.0	0.0
Internal Fluid				
density, ρ	rhof0	1000	1000	1000
Bulk Modulus, K	kf0	2.25×10^{9}	2.25×10^{9}	2.25×10^{9}
viscosity, η	eta0	0.001	0.001	0.001
Others				
	dist	0.45	0.45	0.45
	hash	1	1	1
	nstart	0	0	0
	nend	75	75	75
	exp	1	1	1
	exp0	1	1	1
	nangle	361	361	361
	nfreq	5	5	5
	freqmin	30,000	30,000	30,000
	dfreq	30,000	30,000	30,000

Appendix C
Input to Kargl's Progam: Rigid Solid Case

Parameter	Name	Rigid Sphere
Host (Water)		
density, ρ	rho	1000
Bulk Modulus, K	ks	$(-2.25 \times 10^{9}, 0.0)$*
Shear Modulus, N	emu	$(-2.25 \times 10^{3}, 0.0)$*
porosity, P	beta	0.999999
permeability, k	kd	1.0
min wave number	x1min	0
max wave number	x1max	50
Rigid Sphere		
radius	radius	0.332
density, ρ	rho0	100,000
Bulk Modulus, K	ks0	$(-2.25 \times 10^{13}, 0.0)$*
Shear Modulus, N	emu0	$(-8.44 \times 10^{12}, 0.0)$*
porosity, P	beta0	0.000001
permeability, k	kd0	1×10^{-12}
Exterior Fluid		
density, ρ	rhof	1000
Bulk Modul, K	kf	2.25×10^{9}
viscosity, η	eta	0.0
Internal Fluid		
density, ρ	rhof0	100,000
Bulk Modulus, K	kf0	2.25×10^{13}
viscosity, η	eta0	0.01
Others		
	dist	0.45
	hash	1
	nstart	0
	nend	75
	exp	1
	exp0	1
	nangle	361
	nfreq	5
*complex # format (real,imag)	freqmin	30,000
	dfreq	30,000

LIST OF REFERENCES

(Baker, 1986): S. R. Baker, Sound Propagation in a Superfluid Helium Filled Porous Solid: Theory and Experiment, Diss. UCLA, 1986.

(Berryman, 1980): J. G. Berryman, "Confirmation of Biot's Theory", Appl. Phys. Lett., **37**, 382-384, 1980.

(Biot 1956a): M. A. Biot, "Theory of Propagation of Elastic Waves in a Fluid-Saturated Porous Solid. I. Low-Frequency Range", J. Acoustic. Soc. Am., **28**, 168, 1956.

(Biot 1956b): M. A. Biot, "Theory of Propagation of Elastic Waves in a Fluid-Saturated Porous Solid. II. Higher Frequency Range", J. Acoustic. Soc. Am., **28**, 179, 1956.

(Biot 1962a): M. A. Biot, "Mechanics of Deformation and Acoustic Propagation in Porous Media", J. Acoustic. Soc. Am., **33**, 1482, 1962.

(Biot 1962b): M. A. Biot, "Generalized Theory of Acoustic Propagation in Porous Dissipative Media", J. Acoustic. Soc. Am., **34**, 1254, 1962.

(Brown, 1991): D. A. Brown, Optical Interferometric Acoustic Sensors Using Ellipsoidal Shell Transducers, Diss. Naval Postgraduate School, 1991.

(Garrett, 1990): S. L. Garrett, "Resonant Acoustic Determination of Elastic Moduli", J. Acoustic. Soc. Am., **88**, 1990.

(Johnson and Plona, 1982): D. L. Johnson and T. J. Plona, "Acoustic Slow Waves and the Consolidation Transition", J. Acoustic. Soc. Am., **72**, 1982.

(Kargl and Lim, 1993): S. G. Kargl and R. Lim, "A Transition Matrix Formalism for Scattering in Homogeneous, Saturated, Porous Media", J. Acoustic. Soc. Am., **94**, pp. 1527-1550, 1993.

(Kinsler, et. al.): L. E. Kinsler, A. R. Frey, A. B. Coppens, J. V. Sanders, Fundementals of Acoustics, Third Edition, Wiley, New York, 1982.

(Mayes et. al., 1986): M. J. Mayes, P. B. Nagy, L. Adler, B. P. Bonner, R. Streit, " Excitation of Surface Waves of Diffferent Modes at Fluid-Porous Solid Interface", J. Acoustic. Soc. Am., **79**, 1986.

(Means and Parcher): Physical Properties of Soils, R. E. Means and J. V. Parcher, Charles E. Merrill Books Inc., Columbus, Ohio, 1964.

(Morse): P. M. Morse, Vibrations and Sound, American Institue of Physics, 1976.

(Moses): A. J. Moses, The Practicing Scientist's Handbook, Van Nostrand Reinhold Co, New York, 1978.

INITIAL DISTRIBUTION LIST

1.	Defense Technical Information Center Cameron Station Alexandria, VA 22304-6145	2
2.	Library Code 052 Naval Postgraduate School Monterey, CA 93943-5002	2
3.	Department of the Navy Attn: PMS-407 Naval Sea System Command 2531 National Center Building 3 Washington, DC 20362-5165	1
4.	Commander Attn: Doug Todoroff Naval Coastal System Station Panama City, FL 32407	3
5.	Commanding Officer Naval Undersea Warefare Center Detachment New London, CT 06320-5594	1
6.	Steven R. Baker, Code PH/BA Naval Postgraduate School Monterey, CA 93943-5002	2
7.	Oscar B. Wilson, Code PH/WL Naval Postgraduate School Monterey, CA 93943-5002	1
8.	Dr. David L. Johnson Schlumberger-Doll Research Old Quarry Road Ridgefield, CT 06877-4108	1
9.	Lieutenant Ted W. L. Huskey 503 North Main Street Hinesville, GA 31313	2

DUDLEY KNOX LIBRARY
NAVAL POSTGRADUATE SCHOOL
MONTEREY CA 93943-5101

DUDLEY KNOX LIBRARY
3 2768 00307286 9